

**EVIDENCE FOR IRON-DEPENDENT ANAEROBIC AMMONIUM OXIDATION
TO NITRATE (FEAMMOX) IN DEEP-SEA SEDIMENTS**

**A Thesis
Presented to
The Academic Faculty**

By

Nicole Kiriazis

**In partial fulfillment
Of the Requirements for Degree
Master of Science in Earth and Atmospheric Sciences**

Georgia Institute of Technology

December 2015

Copyright © Nicole Kiriazis 2015

Evidence For Iron-Dependent Anaerobic Ammonium Oxidation to Nitrate (Feammox) In
Deep-Sea Sediments

Approved by:

Dr. Martial Taillefert, Advisor
School of Earth and Atmospheric Sciences
Georgia Institute of Technology

Dr. Joel Kostka
School of Biology
Georgia Institute of Technology

Dr. Yuanzhi Tang
School of Earth and Atmospheric Sciences
Georgia Institute of Technology

Date Approved: 12/03/2015

ACKNOWLEDGEMENTS

I would like to thank my advisor, Dr. Martial Taillefert, for all of his support and feedback over the past few years. I would also like to thank my committee members Dr. Joel Kostka and Yuanzhi Tang for their support and recommendations.

Additionally, I would like to thank Dr. Jordon Beckler and our collaborators on the Congo Lobe cruise, including Dr. Christophe Rabouille, Cecile Cathalot (IFREMER), Dr. Panagiotis Michalopoulos (Hellenic Center for Marine Research), and Dr. Rudolph Corvaisier (IUEM). I would also like to thank the funding from the National Science Foundation Chemical Oceanography program that made this research possible.

I would also like to thank my lab mates in the Taillefert lab group for their support and advice: Dr. Kate Salome, Keaton Belli, Eryn Eitel, and Shannon Owings. I would also like to thank Emily Saad for her assistance with the ammonium methods. I would like to thank the Department of Earth and Atmospheric Sciences for supporting me with a teaching assistantship.

Lastly, I want to thank my friends and family for all of their love and support, especially my parents, Matthew and Mary Kiriazis.

TABLE OF CONTENTS

ACKNOWLEDGEMENTS	iii
LIST OF TABLES	vi
LIST OF FIGURES	vii
CHAPTER 1: INTRODUCTION	1
1.1 The Nitrogen Cycle	1
1.2 Manganese and Nitrogen Redox Reactions	4
1.3 Nitrate Dependent Iron Oxidation	5
1.4 Anaerobic nitrification coupled to iron reduction	6
1.5 Summary and Objectives	8
CHAPTER 2: METHODS	10
2.1 Study Site Background	10
2.2 Core Collection and Processing	12
2.3 Incubations	13
2.4 Analytical Techniques	14
2.4.1: Depth profiles of the main redox species and pH in intact sediment cores....	14
2.4.2: Analyses of pore water and solid samples	16
2.5 Thermodynamic Calculations	17
2.6 MATSEDLAB Model	18
CHAPTER 3: RESULTS	20
3.1 Congo Lobe sediment core profiles	20
3.2 Sediment incubations	29
CHAPTER 4: DISCUSSION	34
4.1 Iron reduction in Congo Lobe Sediments	34

4.2 Anaerobic Nitrification in the Congo Lobe sediments	35
4.3 Thermodynamics of Feammox.....	37
4.4 Evidence for Anaerobic Nitrification from Sediment Incubations	40
4.5 Evidence for Anaerobic Fe(II) Oxidation in the Sediment incubations	44
4.6 Diagenetic modeling of the Congo Lobe sediments and Feammox	49
CHAPTER 5: CONCLUSIONS	52
APPENDIX A.....	54
APPENDIX B	57
Results of first incubations	57
REFERENCES	61

LIST OF TABLES

Table 1: Depth Integrated Concentrations (mol/L) of Dissolved O₂, NO_x⁻, DIC, Fe(II), Fe(III), and ΣPO₄³⁻, Average pH, and Relative Ratio of Ascorbate/Dithionite-Extractable Iron Oxides (A/D) in Sediment from CoL A, CoL B, CoL C, CoL F, and CoL E. The Speciation of Iron Was Measured Both Electrochemically (EC) and in the Pore Waters After Extraction (PW). The pH Represents the Average pH Measured Electrochemically in Each Sediment Core. Ascorbate and Dithionite Iron Were Measured in the Same Sediment After Pore Water Extractions. (ND=not determined.) (*NO_x⁻ is From MTB-6 as it was not Measured in MTB-9 and Both MTB-9 and MTB-6 Were From the Same Location). 28

Table 2: Coupling of Iron Reduction to Ammonium or Nitrite Oxidation and ΔG_r Calculations in the Conditions of the Congo Lobe CoL A Sediments. The following conditions were used: pH = 7.4, [Fe²⁺] = 1 μM, [NO₃⁻] = 1 μM, [NO₂⁻] = 1 μM, [NH₄⁺] = 100 μM, pN₂ = 0.718 atm, pN₂O = 1E-9 atm 40

Table 3: Coupling of Iron Oxidation to Nitrate or Nitrite Reduction and ΔG_r Calculations in the Conditions of the Congo Lobe CoL A Sediments. The following conditions were used: pH = 7.4, [Fe²⁺] = 600 μM, [NO₃⁻] = 100 μM, [NO₂⁻] = 1 μM, [NH₄⁺] = 1 μM, pN₂ = 0.718 atm, pN₂O = 1E-9 atm. 47

Table A 1: Heterotrophic Processes in MATSEDLAB. F[species] Represents the Fraction of Natural Organic Matter Remineralized by Each Component Assuming Michaelis-Menten Kinetics. Denitrification, Iron Reduction, and Sulfate Reduction, are Inhibited by Dissolved Oxygen, Nitrate, and/or Iron Oxides According to a Non-Linear Term Function of the Concentration of Each Inhibitor and an Inhibition Constant (K^I). accel=acceleration factor for aerobic respiration. 54

Table A 2: Complete List of the Secondary Reactions Implemented in the 1D Reactive Transport Model MATSEDLAB and Their Kinetic Formulation. 55

Table A 3: Complete List of Constants Used in MATSEDLAB. M=fit to model data. L=literature: 1) Couture et al., 2010, 2) Wang and Van Capellen 1996,3) Millero and Schreiber 1982, 4) Stumm and Morgan, 1996, 5) Rickard, 2006, 6) Strous et al., 1999.. 56

LIST OF FIGURES

Figure 1: Overview of the nitrogen biogeochemical cycle. Arrows in black represent the classical nitrogen cycle (Thorneley et al., 1978; Froelich et al., 1979; Devol, 1991; Costa et al., 2006). Arrows in green represent new developments within the last 20 years (Mulder et al. 1995; Thamdrup and Dalsgaard, 2002; An and Gardner, 2002). Orange arrows represent the potential couplings between nitrogen and metal cycling (Luther et al., 2007; Straub et al., 1996; Clement et al., 2005)..... 3

Figure 2: Map of Congo Lobe stations a) relative to the African coast and b) bathymetric profiles of lobe complexes. All sites are approximately 800 km offshore from the Congo Estuary by about 5000 m of water depth. Red color represents a depth of -4354 m and the blue represents a depth of -5110 m. 12

Figure 3: Geochemical profiles in the sediment of CoL A MTB-2. Depth is shown in mm, where 0 represents the sediment-water interface (SWI). Panel a) shows dissolved O_2 (μM) in gray, NO_x^- (μM) in pink, and Fe^{2+} (μM) from voltammetry in teal. Panel b) shows pH in black and org-Fe(III) (nA) in open red squares. Panel c) shows dissolved orthophosphates in dark blue solid pentagons, total dissolved Fe as a blue line, dissolved Fe(II) in dark red circles, and dissolved Fe(III) calculated from the difference in total dissolved Fe and dissolved Fe(II) in open red circles. Panel d) shows DIC in black diamonds, ascorbate-reactive iron oxides in red, and dithionite-reactive iron oxides in purple. Error bars represent the standard deviations between replicate analyses, except for the speciation of dissolved Fe and dissolved orthophosphates for which it represents analytical errors..... 22

Figure 4 : Comparison of the depth profiles of NO_x^- , dissolved Fe(II), and dissolved O_2 at different stations along the Congo Lobes: a) CoL A (MTB-2), b) CoL A (MTB-3), c) CoL A (MTB-13), d) CoL C (MTB-6), e) CoL F (MTB-5), f) CoL B (MTB-12), g) CoL E (MTB-14)..... 24

Figure 5: DIC as a function of dissolved ammonium concentrations observed at CoL A. The red line represents a C:N ratio of 15.2 with a bottom water concentration of 2.3 mM DIC ($R^2=0.961$)..... 27

Figure 6: Fe(II), NH_4^+ , and NO_3^- as a function of time in sediment incubations (from CoL A bulk sediments) amended with a) 0, b) 10, c) 50, d) 100 μM , e) 200, f) 500, g) 1000, and h) 2000 μM NH_4^+ . Error bars represent the standard deviation between two replicate incubations. Dashed lines in b-h represent the unamended live control to examine eventual increase in production or consumption of each species..... 32

Figure 7: Correlation between depth-integrated dissolved Fe(II) and NO_3^- in the sediment cores of the Congo lobe. In general, a positive correlation ($R^2 = 0.73$) is found between the depth-integrated concentrations of Fe(II) and NO_3^- at each station, excluding CoL F. 37

Figure 8: Lineweaver-Burk Plot for nitrate production rates (mol/L/day) as a function of moles of NH_4^+ added. R_{max} and K_m were derived using linear regression ($R^2=0.69$). Error bars represent the standard deviation of the rates..... 43

Figure 9: Percent of Fe(II) production due to Feammox in the sediment incubations as a function of ammonium added. 44

Figure 10: Net nitrate removal ($\mu\text{M}/\text{day}$) in the second phase (days 85-202) for the second incubations as a function of ammonium added. The rates display a positive linear correlation ($R^2=0.673$). Error bars represent the difference in rates between replicates. . 48

Figure 11: Comparison of the diagenetic model (lines) compared with field data from CoL A (symbols): a) O_2 (gray), b) NO_3^- (pink) and NH_4^+ (blue), c) $\text{Fe}(\text{OH})_3$ (purple), d) SO_4^{2-} (black), $\Sigma\text{H}_2\text{S}$ (blue). Dashed lines represent the results without Feammox and anammox in the model..... 51

Figure B 1: Fe(II), NH_4^+ , and NO_3^- as a function of time in the first set of sediment incubations (from CoL A bulk sediments) amended with a) 0, b) 10, c) 50, d) 100 μM , e) 200, f) 500, g) 1000, and h) 2000 μM NH_4^+ . Error bars represent the standard deviation between two replicate incubations. 59

SUMMARY

The coupling of iron and manganese with the biogeochemical cycling of nitrogen is an emerging topic in geomicrobiology. Iron oxidation coupled to nitrate reduction is common in a variety of sediments and several organisms have been isolated. The anaerobic reduction of manganese oxides coupled to the oxidation of ammonium to nitrate has been observed in marine sediments and appears sensitive to the reactivity of the manganese oxides. A comparable process proposed to couple iron reduction to the anaerobic production of nitrate has mostly been observed in riparian soils and anaerobic waste reactors. In this study, geochemical profiles of the main redox species involved in carbon transformation in marine sediments from the Congo Lobe demonstrated a peak in nitrate and/or nitrite approximately 1 to 2 cm below the maximum oxygen penetration depth at different stations along the lobes. Batch reactor incubations with the same sediment amended with increasing concentrations of ammonium revealed that nitrate can be produced anaerobically and that its formation is coupled to the reduction of iron oxides. These incubations also demonstrated that the formation of nitrate in anaerobic sediments promotes its successive removal in a process that is tentatively coupled to the oxidation of reduced iron. A one dimensional reactive transport model that includes all the main diagenetic reactions could not reproduce the formation of the subsurface peak in nitrate unless the anaerobic oxidation of ammonium coupled to iron reduction was added to the set of reactions. These findings indicate that nitrite or nitrate are not only a product of aerobic nitrification in marine sediments and suggest that the importance of denitrification or anaerobic ammonium oxidation to nitrogen gas (anammox) in marine sediments may be controlled by the presence of reactive iron oxides.

CHAPTER 1: INTRODUCTION

1.1 The Nitrogen Cycle

Nitrogen is an essential element to all forms of life, as it is an important part of the structures of many biological molecules (Brandes et al., 2007). Although it is abundant in the atmosphere and hydrosphere under the form of nitrogen gas (N_2), it requires special enzymes to break its triple bond (Thorneley et al., 1978). As a result, most organisms depend on fixed nitrogen species as source of this essential element despite the fact that they constitute less than 0.1% of Earth's total nitrogen (Thamdrup, 2012; Canfield et al., 2010). Fixed nitrogen exists in a range of oxidation states, including ammonium (NH_4^+ , -III), organic nitrogen (-III), nitrous oxide (N_2O , -I/+III), nitric oxide (NO, +II), nitrite (NO_2^- , +III), and nitrate (NO_3^- , +V), which undergo a variety of complex redox transformations driven by both chemical and biological forces (Thamdrup, 2012; Figure 1). Anthropogenic inputs through the Haber-Bosch process and fossil fuel combustion have increased the amount of fixed nitrogen available, likely altering the nitrogen budget in ways that are not fully understood (Canfield et al., 2010).

The classical nitrogen cycle was thought to consist of four processes: nitrogen fixation, assimilation/ammonification, nitrification, and denitrification (Brandes et al., 2007). Nitrogen fixation, the reduction of N_2 to ammonia (NH_3), is carried out by a variety of bacteria and archaea using the nitrogenase enzyme (Thorneley et al., 1978). Ammonium is also produced as by-product during the remineralization of organic matter (Froelich et al., 1979) or through dissimilatory nitrate reduction to ammonium (DNRA), a

process that has been shown to preserve fixed nitrogen in anoxic terrestrial and estuary sediments with high levels of sulfide (Sørensen, 1978 ; An and Gardner, 2002 ; Silver et al., 2001). Aerobic nitrification is carried out by ammonia oxidizing bacteria (AOB) and archaea (AOA) that oxidize ammonium to nitrite, but a separate group of organisms oxidize nitrite to nitrate (Costa et al., 2006). In the classical view, canonical denitrification, where nitrate is reduced to nitrogen gas in suboxic conditions by heterotrophic bacteria, is the most important sink for fixed nitrogen (Devol, 1991; Brandes et al., 2007). However, anaerobic ammonium oxidation (anammox), which consumes ammonium and nitrite to produce dinitrogen without oxygen, has also been shown to contribute significantly to fixed-N loss, especially in marine ecosystems (Mulder et al., 1995; Strous et al., 1999; Thamdrup and Dalsgaard, 2002). Anammox is carried out by anaerobic chemoautotrophs that can tolerate a wide range of environments (Strous et al., 1999; Rysgaard and Glud, 2004; Brandes et al., 2007) and is estimated to account for approximately 21-39% of global N₂ production (Thamdrup, 2012). Interestingly, evidence for anammox in marine sediments is found well below the oxygen and nitrate minima (Jaeschke et al., 2009 and 2010; Brandsma et al., 2011; Hou et al., 2012; Rooks et al., 2012), suggesting that an additional source of nitrite is needed to fuel anammox in deeper sediments.

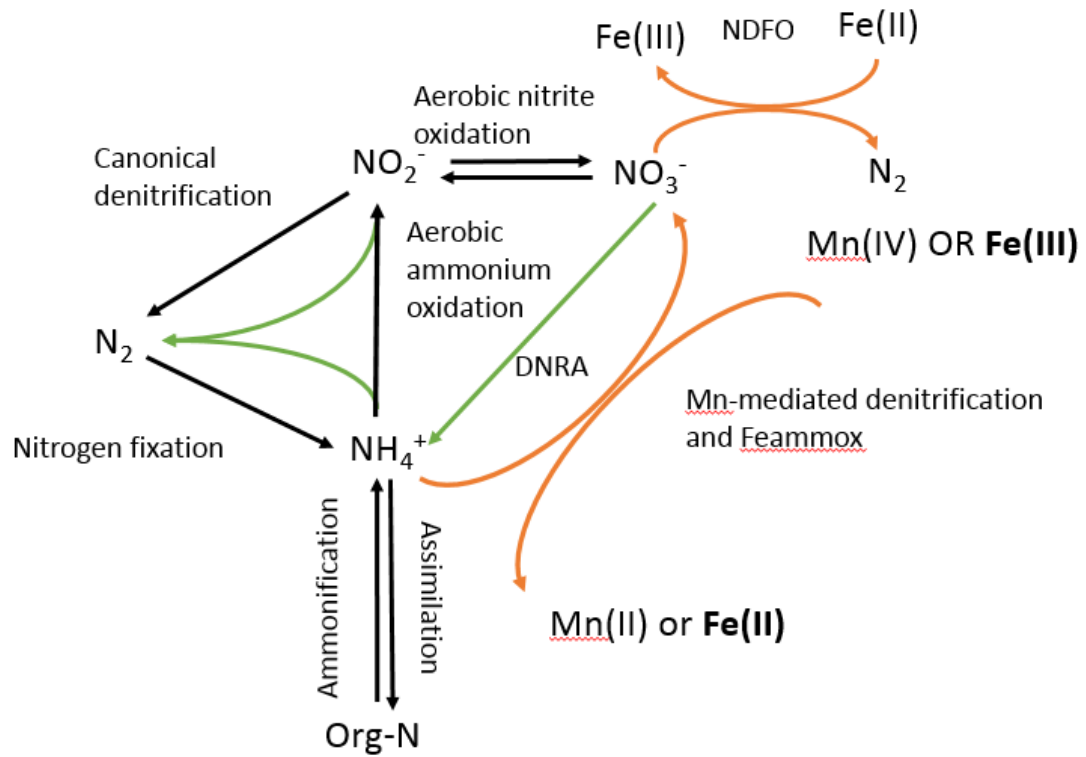


Figure 1: Overview of the nitrogen biogeochemical cycle. Arrows in black represent the classical nitrogen cycle (Thorneley et al., 1978; Froelich et al., 1979; Devol, 1991; Costa et al., 2006). Arrows in green represent new developments within the last 20 years (Mulder et al. 1995; Thamdrup and Dalsgaard, 2002; An and Gardner, 2002). Orange arrows represent the potential couplings between nitrogen and metal cycling (Luther et al., 2007; Straub et al., 1996; Clement et al., 2005).

1.2 Manganese and Nitrogen Redox Reactions

Manganese oxidation and reduction have long been proposed as alternative pathways to nitrification and denitrification (Luther et al., 1997; Hulth et al., 1999). Thermodynamic calculations demonstrated that both Mn(II) oxidation coupled to nitrate reduction to N₂ and manganese oxide reduction coupled to ammonium oxidation to N₂ are thermodynamically favorable (Luther et al., 1997). The consumption of nitrate and nitrite in the presence of MnO₂ and oxygen as well as the buildup of nitrate in comparable Mn-poor sediments were used to propose that in the presence of MnO₂, ammonium is oxidized directly to N₂ and nitrate does not build up in the sediments (Luther et al., 1997). Incubations of marine sediments conducted at increasing concentrations of manganese oxides demonstrated the anoxic production of nitrate and nitrite in proportion to the concentration of manganese oxides (Hulth et al., 1999). More recently, a denitrifying strain isolated from coastal sediments was capable of reducing Mn oxides and producing nitrous oxide in the presence of ammonium but without nitrate, providing indirect evidence of anaerobic nitrification (Javanaud et al., 2011).

Manganese-dependent anaerobic nitrification is not solely dependent on concentrations of manganese in sediments, as incubations of manganese-rich continental margin sediments showed no evidence of manganese-dependent ammonium oxidation (Thamdrup and Dalsgaard, 2000). It has been proposed that anaerobic nitrification coupled to manganese reduction is favored in recently disturbed sediments where freshly formed manganese oxides may be found (Bartlett et al., 2008). Later investigations showed that Mn(III) oxyhydroxides rather than Mn(IV) oxides may be better reactants for

anaerobic nitrification (Anschutz et al., 2005). Indeed, sediment incubations from salt marsh sediments have revealed that many geochemical factors affect anaerobic nitrification coupled to manganese oxides (Lin and Taillefert, 2014). Amendments with NH_4^+ increased nitrification, suggesting that the N:Mn concentration ratio is important to this process. It was also shown that colloidal MnO_2 , with its high specific surface area, was necessary to catalyze anaerobic nitrification. Small additions of NO_3^- or low SO_4^{2-} concentrations were also found to be favorable to this process, suggesting that moderately reducing environments are most favorable to manganese-driven anaerobic nitrification (Lin and Taillefert, 2014). Overall, these findings demonstrate that Mn(IV) oxides may be an important source of anaerobic nitrification, increasing the availability of nitrite and nitrate for denitrification and anammox.

1.3 Nitrate Dependent Iron Oxidation

In a similar fashion, iron has also been proposed to be coupled to the nitrogen cycle, primarily through nitrate dependent iron oxidation (NDFO). Luther et al. (1997) calculated that Fe(II) oxidation could be coupled with nitrate reduction to N_2 , similar to the proposed manganese-driven denitrification. This process, catalyzed by the nitrate reducing enzyme *nar* (Carlson et al., 2013), was first demonstrated in pure and enrichment cultures of heterotrophic denitrifying bacteria from freshwater and brackish waters enriched with Fe(II) and nitrate (Straub et al., 1996; 1998). NDFO has since been found in many freshwater environments, and most of the species isolated are mixotrophs that require an organic carbon source (Weber et al., 2006). Although the majority of anaerobic Fe(II)-driven nitrate reducing bacteria have been found in freshwater or brackish waters, a limited number of aerobic marine iron-oxidizing strains that can

oxidize Fe(II) from solid sources such as pyrite (FeS₂) and basalt may use nitrate as an electron acceptor (Edwards et al., 2003). The primary end-products of nitrate-dependent Fe(II) oxidation are N₂ and the poorly crystalline Fe(III) oxyhydroxide ferrihydrite, but this process has also been shown to form goethite, magnetite, and the highly reactive “green rust”, which contains both Fe(II) and Fe(III) (Straub et al., 1996; Kappler et al., 2005; Kappler et al., 2011). In addition to aqueous Fe(II), pyrite (FeS₂), siderite (FeCO₃), (Edwards et al., 2003), and a biologically reduced form of the phyllosilicate nontronite (Zhao et al., 2013) catalyze nitrate-dependent iron oxidation. In the latter investigation, it was also proposed that Fe(III) during the oxidation process remains sorbed to the Fe(II) mineral to serve as electron shuttle between nontronite and nitrate (Zhao et al. 2013). Whether this reaction is always microbially driven remains unclear (Klueglein and Kappler, 2013), as abiotic reduction of nitrite to N₂ coupled with Fe(II) oxidation to ferrihydrite is thermodynamically favorable even at circumneutral pH (Van Cleemput and Baert, 1983) and nitrite abiotically oxidizes Fe(II) though the reaction is faster at low pH (Kampschreur et al., 2011).

1.4 Anaerobic nitrification coupled to iron reduction

Although a variety of organisms that couple the oxidation of Fe(II) to the reduction of nitrate or nitrite have been identified, less evidence has been reported of the reverse process. It is unclear why a direct coupling between Fe(III) reduction and ammonium oxidation to nitrite (or nitrate), in a process called ‘Feammox’ (Sawayama, 2006), has not been considered more thoroughly, especially given the evidence for manganese-dependent anaerobic nitrification (Hulth et al., 1998; Javanaud et al., 2011; Lin and Taillefert, 2014).

Nitrate and Fe(II) were found to coexist throughout a lake sediment core, suggesting that anaerobic nitrification could be a possibility in this environment (Weber et al., 2006). Anaerobic incubations of forest riparian soils with urea as nitrogen source led to the production of NO_2^- that rapidly disappeared without formation of NO_3^- , and the inverse relationship between total dissolved nitrogen (i.e. excess urea and ammonium) and Fe(II) produced led to the conclusion that iron reduction was coupled to anaerobic ammonium oxidation to nitrite (Clément et al., 2005). Similarly, nitrite production, ammonium oxidation, and the addition of Fe(III) EDTA were linked to the presence of iron reducers of the *Exiguobacterium* genus in an anoxic flow-through reactor containing anaerobically digested waste treatment sludge (Sawayama, 2006). The proportional increase in nitrite and nitrate concentrations observed in an anaerobic wastewater culture exposed to increasing Fe(III) citrate and ammonium concentrations was tentatively explained by Feammox and the ensuing stimulation of anammox (Park et al., 2009). Indeed, the production of $^{29}\text{N}_2$ and $^{30}\text{N}_2$ in soils incubated with $^{15}\text{NH}_4^+$ and exogenous Fe(III) demonstrated that the Feammox process may promote the significant loss of nitrogen via anammox (Yang et al., 2012). This process is proposed to accelerate the loss of fixed nitrogen from highly cultivated rice paddy soils, as poorly crystalline iron oxides are present in higher concentrations in cultivated, compared to uncultivated, soils (Ding et al., 2014). In this particular study, Feammox accounted for 67% of N_2 production in all soils incubated, though only 0.8-4% of total iron reduction was linked to Feammox. The proportion of Fe(III) reduction by Feammox was also inversely correlated with total organic carbon, suggesting that microorganisms are more likely to use ammonium as an electron acceptor for iron reduction in environments with lower organic carbon, such as

leached soils rich in poorly crystalline iron oxides. In a separate study, Feammox in coastal sediments correlated with the intensity of tides, suggesting that areas with high Fe(III) oxides and fluctuating redox conditions could support Feammox in circumneutral pH environments (Li et al., 2015). Finally, a bacterium of the *Acidimicrobiaceae* family that catalyzes Feammox has been enriched from riparian soils in the presence of a solid Fe(III) electron acceptor such as ferrihydrite or goethite only, suggesting that the reaction should be favored in soils and sediments with high iron oxides (Huang and Jaffe, 2015).

1.5 Summary and Objectives

The coupling of iron and manganese with nitrogen redox transformations is an emerging field in geochemistry and microbiology. Iron oxidation coupled to nitrate reduction has been observed in freshwater, brackish, and marine environments and several organisms have been isolated that mediate this process, though the exact biological mechanism is still under debate (Straub et al., 1996 ; Weber et al., 2009 ; Klueglein and Kappler, 2013). The anaerobic oxidation of ammonium coupled to the reduction of manganese oxides has also been observed in marine sediments (Luther et al., 1997; Hulth et al., 1999; Anschutz et al., 2005; Javanaud et al., 2011; Lin and Taillefert, 2014), and one organism responsible for this process has been isolated (Javanaud et al., 2011). This study explores the potential existence of the anaerobic oxidation of ammonium to nitrite or nitrate coupled to the reduction of iron oxides (Feammox) in marine sediments and its potential implications for the nitrogen cycle. Two hypotheses were tested:

Hypothesis 1. The anaerobic oxidation of ammonium to nitrite or nitrate can be coupled to the reduction of iron oxides.

Hypothesis 2. The production of nitrite and nitrate in anaerobic marine sediments promotes their removal via denitrification or anammox.

These hypotheses were tested using iron-rich sediments from the edge of the continental slope of a river-dominated ocean margin (RiOMar). Geochemical measurements obtained as a function of depth at various stations, diagenetic modeling to diagnose our understanding of the main processes regulating the transformation of iron and nitrogen, and anaerobic sediment incubations were combined to examine the existence of iron-dependent anaerobic nitrification in these sediments and its role in the nitrogen cycle.

CHAPTER 2: METHODS

2.1 Study Site Background

River-dominated ocean margin (RiOMar) sediments are dynamic environments that occupy a small area of the world's oceans, but are responsible for a large portion of biogeochemical processes and 90% of global carbon burial (McKee et al., 2004). The largest rivers in terms of freshwater and sediment discharge to the ocean are responsible for 40% of fluvial sediment delivery to the ocean. Sediment deposits from riverine systems contain high concentrations of reactive iron oxides, making iron biogeochemical cycling important in continental margins (Aller et al., 2004; Beckler et al., 2015; Poulton and Raiswell, 2005). The Congo River is 4700 km long and drains an area of 3.7×10^6 km², covering mostly rainforest and savannah areas of low elevation in a wet tropical climate (Babonneau et al., 2002; Dupré et al.; 1996) before discharging in the equatorial Atlantic Ocean (Figure 2a). The Congo River is the second-largest river in the world in terms of fluid discharge, but has a considerably lower sedimentary discharge rate compared to the Amazon and other large rivers (Babonneau et al., 2002). The Congo River submarine canyon cuts through the continental shelf and slope, reaching a maximum depth of 1300 m and width of 15 km near the shelf break (Babonneau et al., 2002). The canyon transitions into a less steep, relatively straight active channel that terminates with the distal lobe complex examined in this study. The direct connection between the estuary and the submarine canyon has led to active turbidity currents throughout the Holocene, unlike other large rivers such as the Amazon and Mississippi

(Savoie et al., 2009). The source of these currents is uncertain, but may be due to a combination of hyperpycnal flows, sediment overload at the canyon head, and longshore currents (Savoie et al., 2009). McKee et al., (2004) classify the burial of fine-grained RiOMar sediment according to the energy and geomorphology of the delta, describing the Congo River depocenter as a system where more than 10% of terrigenous sediment is buried past the shelf break due to the canyon funneling sediment seaward. In contrast, the Amazon River generates a higher sediment load to its continental margin, but the terrigenous sediments have been deposited on the continental shelf during the Holocene and other interglacial periods, leaving its fan inactive (Jegou et al., 2008). The Congo River deep sea fan is thought to play an important role in the global carbon and silica cycles due to the high accumulation and rapid transport of amorphous silica (Raimonet et al., 2015). The lobe complex contains approximately 3% natural organic matter of terrestrial origin mainly, which is unique for the deep sea (Rabouille et al., 2009). The high input of terrestrial organic matter, along with the high sedimentation rates recorded (1.9 cm/yr) create an organic carbon burial environment comparable to a river delta (Rabouille et al., 2009; McKee et al., 2004). As anaerobic nitrate production has been observed in poorly crystalline iron-rich sediments (Yang et al, 2012; Ding et al., 2014; Li et al., 2015; Huang and Jaffe, 2015), a RiOMar such as the Congo River deep sea fan presents great potential to study the Feammox process.

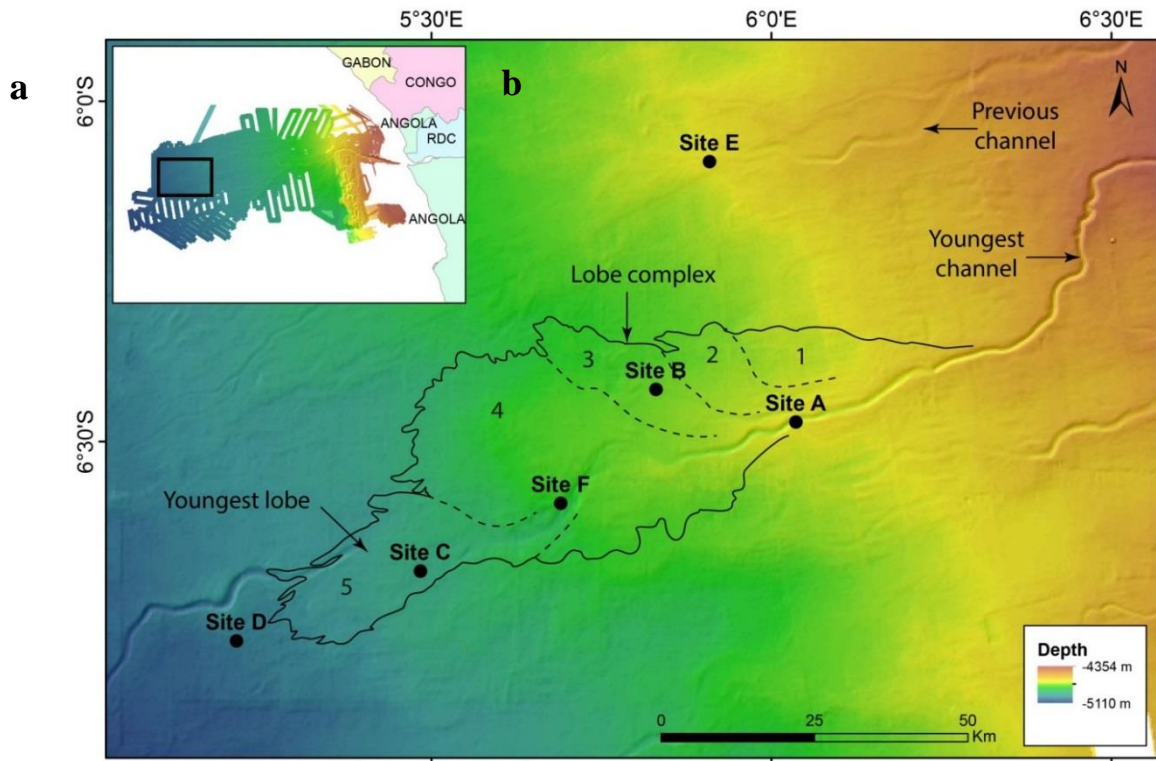


Figure 2: Map of Congo Lobe stations a) relative to the African coast and b) bathymetric profiles of lobe complexes. All sites are approximately 800 km offshore from the Congo Estuary by about 5000 m of water depth. Red color represents a depth of -4354 m and the blue represents a depth of -5110 m.

2.2 Core Collection and Processing

Sediment cores were collected using a multi-corer on the banks or levees of the Congo Lobe stations CoL A, CoL B, CoL C, CoL E, and CoL F in the Congo River deep sea fan (Figure 2b) during a research cruise on the *N/O Pourquoi Pas?* (IFREMER) in December 2011. The presently active Congo deep sea fan is located approximately 800 km west of the mouth of the Congo River delta at a depth of approximately 4500-5100 m.

CoL A lays at the entry point of the lobe complex near the bottom of the slope and is the oldest lobe channel, whereas CoL C and D, positioned the farthest from the slope represent the youngest lobe. CoL F is an intermediate station in the lobe complex, while CoL E represents an extinct channel of unknown age (Figure 2).

For this study, a total of 8 sediment cores representing 5 stations along the Congo Lobe deep sea fan were first profiled over ~20 cm and at 4° C using non-invasive voltammetric microelectrodes (Taillefert et al., 2000; Luther et al., 2008). The same cores were sectioned under N₂ atmosphere in a walk-in refrigerator (4°C), and the pore waters were extracted from each section by centrifugation at 3000 rpm for approximately 10 minutes and immediately filtered (0.2 µm Puradisc filters, Millipore) under N₂ atmosphere at the same temperature. Pore water samples were then analyzed for Fe(II), total dissolved iron, dissolved inorganic carbon (DIC), orthophosphate (ΣPO_4^{3-}), and nitrite+nitrate (ΣNO_x^-) onboard ship within 8 hours after sampling. The remaining sediments were frozen at -20°C for solid phase extractions at Georgia Tech.

2.3 Incubations

Bulk sediment from the CoL A (MTB-13) 1.5-5 cm depth interval was used to conduct batch reactor sediment incubations. An aliquot of homogenized bulk sediment (1.5-2.5 g) were added to 25 mL Hungate tubes filled with Synthetic Ocean Water (SOW) degassed with argon and immediately sealed. The SOW had a composition of 0.42 M NaCl, 54.6 mM MgCl₂·6H₂O, 28.8 mM Na₂SO₄, 10.5 mM CaCl₂·2H₂O, 9.39 mM KCl, 2.3 mM NaHCO₃, 0.84 mM KBr, 48.5 µM H₃BO₃, 71.5 µM NaF, and 63.8 µM

SrCl₂, and 10 μM NaH₂PO₄ (Morel et al., 1979). As solid phase analysis of iron oxides showed that amorphous iron oxides were abundant in these sediments, ammonium was hypothesized to be the main limiting factor in the Feammox reaction. A series of seven incubations was conducted in duplicate with increasing concentrations of NH₄⁺. To this end, a degassed NH₄Cl solution was added to each reactor at the beginning of the incubation to reach final added concentrations of 10, 50, 100, 200, 500, 1000, and 2000 μM to investigate its effect on the process. An unamended live control was also conducted to which no ammonium was added. All treatments were mixed in sealed Hungate tubes and kept in the dark at room temperature on rotary wheels for up to 200 days. Aliquots of 1 mL were taken at 0, 20, 40, 85, and 202 days using sterile 1 mL syringes. Half of each aliquot was filtered onto 0.2 μm nitrocellulose membrane filters (Millipore) and frozen immediately after collection until analysis for ammonium, nitrite, and nitrate. The remainder was unfiltered and extracted with 0.5 M HCl for 48 hours until analysis of total Fe(II), which includes dissolved Fe(II), adsorbed Fe(II), and any carbonate minerals or Fe(II) sulfide minerals that may have precipitated during the incubations. To ensure the sealed reactors were not exposed to oxygen from the atmosphere during these long incubations, an abiotic control consisting of SOW amended with 600 μM of Fe(II) chloride was incubated under the same conditions and sampled according to the same protocol.

2.4 Analytical Techniques

2.4.1: Depth profiles of the main redox species and pH in intact sediment cores

Dissolved oxygen ($O_{2(aq)}$), Fe(II), Mn^{2+} , ΣH_2S , $FeS_{(aq)}$, and soluble organic-Fe(III) complexes were determined as a function of depth in intact sediment cores within 30 minutes after recovery using gold/mercury (Au/Hg) voltammetric microelectrodes (Taillefert et al., 2000; Luther et al., 2008). For these measurements, a three electrode system, including Au/Hg microelectrodes as working electrode, an Ag/AgCl reference electrode, and a Pt counter-electrode were used with a DLK-100 potentiostat and a MAN-EX1 micromanipulator (Analytical Instrument Systems, Inc) both controlled by a laptop computer. In addition, a pH minielectrode (Microelectrodes, Inc.) was deployed alongside the Au/Hg microelectrode (within 1 cm) and monitored directly with the DLK-100 potentiostat. Under this configuration, the pH and voltammetric electrodes were lowered from the overlying waters to as deep as 20-25 cm in the sediment in increments varying between 1 and 5 mm, while the counter and reference electrodes were maintained in the overlying waters during measurements. Dissolved oxygen was measured by linear sweep voltammetry (LSV), while Fe(II), Mn(II), ΣH_2S , $FeS_{(aq)}$, and soluble organic-Fe(III) complexes were measured by cathodic square wave voltammetry (CSWV) according to standard procedures for marine sediments (Meiggs and Taillefert, 2011). Voltammetric microelectrodes were calibrated for $O_{2(aq)}$ in the overlying waters, using salinity and temperature to calculate oxygen saturation (Luther et al., 1998). In addition, voltammetric microelectrodes were calibrated for Mn(II) before and after deployments, and the pilot ion method was used to calibrate for Fe(II) and ΣH_2S (Brendel and Luther, 1995; Taillefert et al., 2000). The composition of the soluble organic-Fe(III) and $FeS_{(aq)}$ complexes remains unknown such that these species cannot be quantified and are, therefore, reported in current intensities (Taillefert et al., 2007). Voltammetric profiles

were analyzed using a semi-automated program (Bristow and Tallefert, 2008). The pH minielectrode was calibrated using a TRIS standard in NaCl 0.54 M and the potential and temperature were recorded to calculate the pH according to Nernst Law.

2.4.2: Analyses of pore water and solid samples.

Dissolved inorganic carbon (DIC) and orthophosphates (ΣPO_4^{3-}) were quantified in the pore waters of each sediment core by flow injection analysis (Hall and Aller, 1992) and the molybdenum blue method respectively (Murphy and Riley, 1962). Total dissolved iron (Fe_T) and dissolved Fe(II) were quantified in the same pore waters using the ferrozine method with and without hydroxylamine (Stookey, 1970; Lovley and Phillips, 1987). The sum of nitrate and nitrite (NO_x^-) was also quantified using the cadmium reduction method with detection of nitrite by spectrophotometry (Jones, 1984). Parallel ascorbate and dithionite extractions on the sectioned and centrifuged sediments were conducted to determine the amorphous fraction of iron oxides and the total iron oxides (Kostka and Luther, 1994). In parallel, a sample of sediment from each slice was dried for several days at 45°C to normalize the iron oxide concentrations to the dry weight of sediment. Finally, total Fe(II) extracted from the incubations was measured using the ferrozine method as above. Ammonium from the incubated pore waters was quantified using the indophenol blue method (Strickland and Parsons, 1972), whereas nitrate and nitrite were quantified in the same undiluted samples by UV absorbance at 215 nm after separation by high-performance liquid chromatography (HPLC). The HPLC method used a 20 μl sample loop to introduce the sample onto a 150 x 0.4 mm Metrosep A Supp 5 anion exchange column with guard column (Metrohm) using a 54

mM NaCl eluent at 0.7 ml min⁻¹ (Beckler et al., 2014). To compare the geochemistry of the different sediment cores, depth-integrated concentrations of dissolved species were calculated by summing the number of moles of each species in each depth interval and normalizing to the total volume of pore waters according to Equation 1:

$$Z = \frac{\sum_{i=1}^n \phi C_i V_i}{\sum_{i=1}^n V_i} \quad (\text{Eq. 1})$$

where C_i is the concentration of a species in slice i in mol/L (for solute species) or in $\mu\text{mol/g}$ dry wt. sediment (for solid species), V_i is the volume of slice i in L, and $\phi = \phi$ for solute species and $\phi(1-\rho)$, where ϕ equals the porosity of slice i and ρ equals the average bulk density of 2.65 g/cm³. The average pH of all depths for each core was also calculated and presented in Table 1. The solid phase data are presented as the depth-integrated ascorbate and dithionite reactive iron oxide concentrations as well as a ratio of ascorbate-reactive iron oxides to dithionite-reactive iron oxides as a percentage.

2.5 Thermodynamic Calculations

To assess the thermodynamic favorability of the reactions involving the redox transformations of iron and nitrogen, the Gibbs free energy (ΔG_r) for the oxidation of Fe(II) by nitrite and nitrate and the reduction of iron oxides by ammonium and nitrite to various forms of nitrogen products were calculated under the geochemical conditions found in the Congo Lobe sediments of CoL A (MTB-2). Since temperature and pressure could significantly affect the ΔG^0 at the ocean floor (5000 m depth), the program SUPCRT92 was used to compute these values (Johnson et al., 1992). Activity coefficients were adapted from Millero and Schreiber (1982).

2.6 MATSEDLAB Model

Diagenetic processes were analyzed using the model MATSEDLAB (Couture et al., 2009), a one-dimensional reactive transport model implemented in MATLAB that accounts for the degradation of natural organic matter by dissolved oxygen, iron oxides, and sulfate, the abiotic oxidation of Fe(II) and dissolved sulfide by dissolved oxygen, the precipitation of FeS, and the abiotic reduction of iron oxides by dissolved sulfide. The model was modified to add nitrate and ammonium species, aerobic nitrification, canonical denitrification, anammox, the precipitation of siderite (FeCO₃), and the Feammox reaction. A list of the complete set of reactions, their kinetic rate laws, and the constants used is provided in the Appendix (Tables A1-3). In addition, the model was modified to account for the sedimentation rate ($w = 1.9$ cm/yr) and organic matter content of the Congo Lobe environment (Rabouille et al., 2009). In these deep sediments, advection was assumed to be negligible (6×10^{-9} cm s⁻¹) and diffusion molecular. Diffusion coefficients of anions (SO₄²⁻, NO₃⁻, HS⁻) and cations (Fe(II), NH₄⁺) were calculated from empirical relationships that are function of the temperature (Boudreau, 1997). The molecular diffusion coefficient of dissolved oxygen was calculated at the salinity (36 ppt), temperature (4°C), and pressure (500 atm) of the site according to:

$$D^0 = 4.72 * 10^{-9} \frac{T}{\mu V_b^{0.6}} \quad (\text{Eq. 2})$$

where D^0 is the molecular coefficient of O_{2(aq)} [cm² s⁻¹], T is the absolute temperature [K], μ is the dynamic viscosity of seawater at the temperature, pressure, salinity of the site [poise], and V_b is the molar volume of molecular oxygen [cm³ l⁻¹] (Boudreau, 1997). The rate constant of organic matter decay with depth was found by fitting organic carbon

data from CoL A to the analytical solution of the 1-D diagenetic equation (Van Genuchten 1981). The pH was set to 7.0 and the DIC to 2.3 mM, equivalent to the bottom water concentration at CoL A. A C:N ratio of 15.5, representing the average composition of particulate organic carbon at the site, was used to predict the fraction of ammonium released during the remineralization of organic carbon. The bulk density was set to 2.6 g/cm³ and a constant porosity of 0.977 was used for calculations involving solid species. Field data from the Congo Lobe CoL A (MTB-13 and MTB-2) was used to compare experimental and calculated concentrations of O₂, Fe(OH)₃, SO₄²⁻, Fe(II), H₂S, FeS, NO₃⁻, and NH₄⁺. Boundary conditions for solute species (O₂, SO₄²⁻, Fe(II), H₂S, NO₃⁻, NH₄⁺) were set at the bottom water concentrations found in the field data for CoL A (O₂=0.19 μmol/cm³, NO₃⁻=0.02 μmol/cm³, all others 0). For Fe(OH)₃, the boundary condition was set as a flux term that fits the profile of total iron oxides found by dithionite extraction. Kinetic constants from known reactions were taken from the literature (Millero and Schreiber 1982, Stumm and Morgan, 1996; Wang and Van Capellen, 1996; Rickard, 2006; Couture et al., 2010). When appropriate, rate constants were optimized by hand to fit the data (Table A3).

CHAPTER 3: RESULTS

3.1 Congo Lobe sediment core profiles

Typical depth profiles of dissolved and solid constituents obtained in the Congo Lobe sediments are shown in Figure 3 for CoL A (MTB-2). Dissolved oxygen decreased from saturation in the overlying waters to depletion at approximately 1 cm below the sediment-water interface (Figure 3a). Nitrate and nitrite (NO_x^-) decreased initially from $\sim 28 \mu\text{M}$ near the sediment-water interface to just above detection limit ($\sim 2 \mu\text{M}$) about a centimeter below the oxygen penetration depth. NO_x^- then rebounded between 2 and 4.5 cm to a concentration of $100 \mu\text{M}$ before decreasing to a minimum of $4 \mu\text{M}$ at 7 cm. Fe(II) measured by voltammetry was first detected at 3 cm and increased regularly with depth to a stable concentration of approximately $700 \mu\text{M}$ after 8 cm (Figure 3a). Voltammetric currents for soluble organic-Fe(III) complexes increased with depth and mirrored the profile of Fe(II) (Figure 3a and b). The pH decreased rapidly from 8.2 in the overlying water to 7.4 at about 1 cm, decreased gently to 7.3 at about 6 cm, then seemed to rebound slightly deeper to stabilize around 7.4 below 10 cm (Figure 3b). Neither Mn(II), dissolved sulfides, nor $\text{FeS}_{(\text{aq})}$ were detected in these cores, and no black precipitate or sulfidic odor was observed during core processing. Total dissolved Fe was first detected around 2 cm, increased rapidly to $700 \mu\text{M}$ at 4 cm and reached a peak concentration of 1 mM at depth (Figure 3c). Dissolved Fe(II) followed the same pattern and reached a concentration of $800 \mu\text{M}$ at depth. Dissolved Fe(III), calculated as the difference between total dissolved Fe and dissolved Fe(II), was first detected at 3 cm then remained around $200 \mu\text{M}$

throughout the core (Figure 3c). Pore water orthophosphates were generally low ($<2 \mu\text{M}$) at all depths (Figure 3c), while DIC increased continuously with depth from 3 to 6 mM (Figure 3d). Finally, ascorbate-extractable iron oxides were dominant throughout the core, decreasing from a peak of $672 \mu\text{mol Fe/g dry weight}$ in the oxygenated layers ($\leq 2 \text{ cm}$) to $250 \mu\text{mol Fe/g dry weight}$ at 13 cm depth (Figure 3d). Dithionite-extractable iron oxides followed the profile of ascorbate-extractable iron oxides, albeit at slightly higher concentrations ($642 \mu\text{mol Fe/g dry weight}$ maximum and $289 \mu\text{mol Fe/g dry weight}$ minimum), suggesting the majority of the sediment consisted of highly reactive amorphous iron oxides. Porewater orthophosphates increased from $< 1 \mu\text{M}$ at the surface to a maximum concentration of $4.67 \mu\text{M}$ at depth.

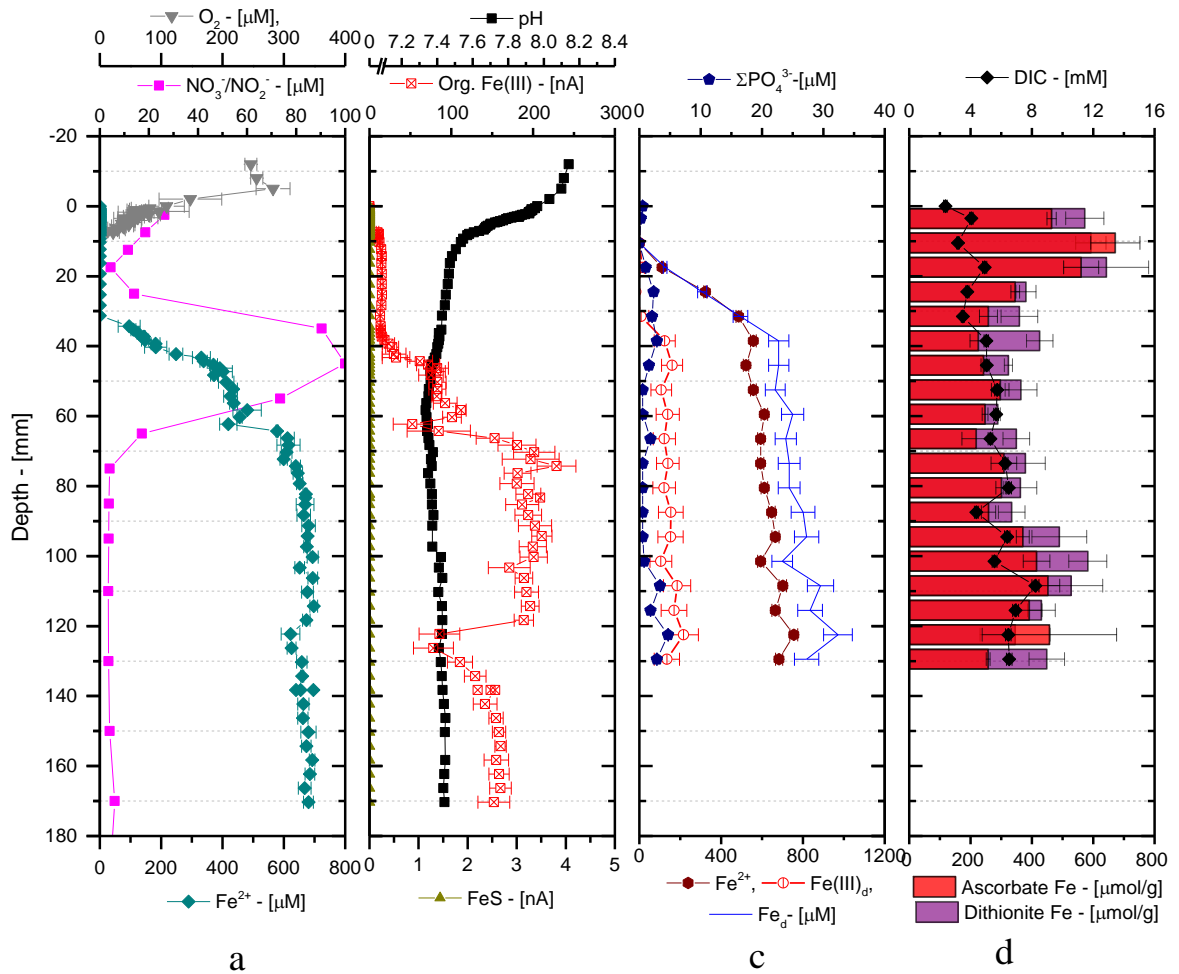


Figure 3: Geochemical profiles in the sediment of CoL A MTB-2. Depth is shown in mm, where 0 represents the sediment-water interface (SWI). Panel a) shows dissolved O_2 (μM) in gray, NO_x^- (μM) in pink, and Fe^{2+} (μM) from voltammetry in teal. Panel b) shows pH in black and org-Fe(III) (nA) in open red squares. Panel c) shows dissolved orthophosphates in dark blue solid pentagons, total dissolved Fe as a blue line, dissolved Fe(II) in dark red circles, and dissolved Fe(III) calculated from the difference in total dissolved Fe and dissolved Fe(II) in open red circles. Panel d) shows DIC in black diamonds, ascorbate-reactive iron oxides in red, and dithionite-reactive iron oxides in purple. Error bars represent the standard deviations between replicate analyses, except for the speciation of dissolved Fe and dissolved orthophosphates for which it represents analytical errors.

A comparison of the depth profiles of dissolved oxygen, NO_x^- , and Fe(II) at all the stations that display a subsurface maximum in NO_x^- is presented in Figure 4. All three CoL A profiles, obtained on the levees north (MTB2 and MTB13) and south (MTB3) of the canyon showed either a gap between oxygen depletion (1 cm) and the onset of NO_x^- production (1.8 to 2.2 cm at MTB-2 and MTB-3) or a small overlap (MTB-13). In addition, peaks in NO_x^- concentrations varying between 80 and 100 μM were detected in each core at this station (Figure 4a-c). These peaks either coincided with the onset of Fe(II) (MTB2) or were immediately above the zone of iron reduction (MTB3 and MTB13). The sediments from CoL C (MTB-6), CoL F (MTB-5), and CoL B (MTB-12) showed similar trends (Figure 4d-f), with gaps between the oxygen penetration depth and the rebound in NO_x^- ranging between 1 cm at CoL C, 0.4 cm at CoL F, and 4.5 cm at CoL B. At these stations, however, NO_x^- reached peak concentrations of 60 μM at CoL C, 7 μM at CoLB, and 5.5 μM at CoL B only, and Fe(II) concentrations were significantly lower than at CoLA. In contrast, the oxygen penetration depth in CoL E, the extinct channel, reached 6 cm, much deeper than at the other stations, and no subsurface accumulation of NO_x^- was observed (Figure 4g). NO_x^- decreased from 25 μM in the first 0.5 cm to a minimum of 1 μM at 8.5 cm.

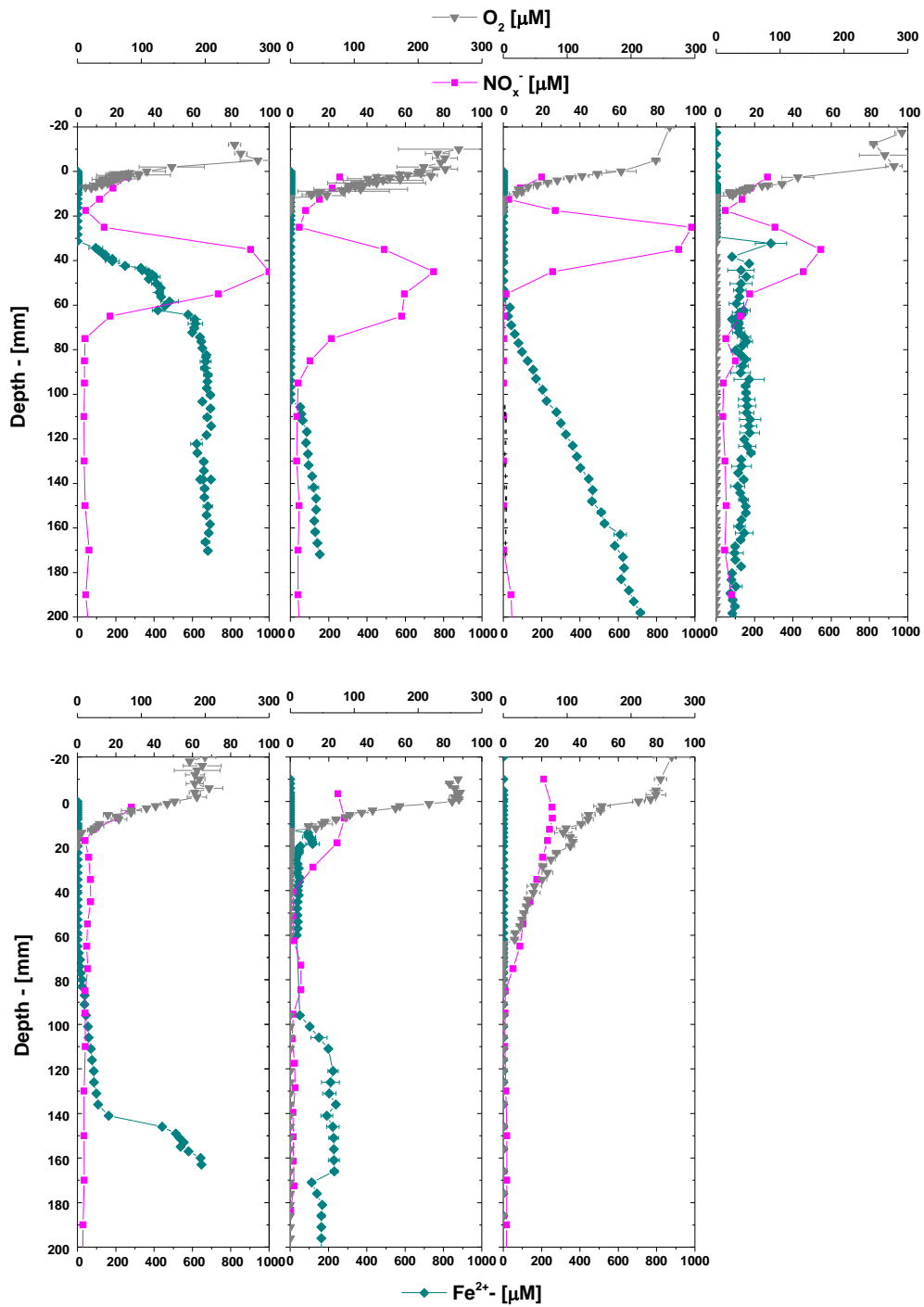


Figure 4 : Comparison of the depth profiles of NO_x^- , dissolved Fe(II), and dissolved O_2 at different stations along the Congo Lobes: a) CoL A (MTB-2), b) CoL A (MTB-3), c) CoL A (MTB-13), d) CoL C (MTB-6), e) CoL F (MTB-5), f) CoL B (MTB-12), g) CoL E (MTB-14).

For comparison, the depth-integrated concentrations of dissolved O₂, NO_x⁻, Fe(II), pH, dissolved Fe(II) and Fe(III), DIC, and ΣPO₄³⁻ from the cores collected at each station are presented in Table 1. Integrated concentrations of dissolved oxygen fluctuated between a minimum of 108 μM at CoL E to a maximum around 200 μM at CoL A. These variations represent changes in oxygen penetration depth as well as changes in respiration rates at the different stations. Although the integrated concentration of dissolved oxygen was much lower at CoL E, it reflected the large oxygen penetration depth (6.2 cm) in the extinct canyon (Figure 4g), indicative of less intense remineralization processes. Comparatively, the oxygen penetration depth at CoL A, B, C, and F were similar (~0.75 to 1.4 cm), indicative of the relatively similar intensity of the processes remineralizing carbon at these stations. In this context, integrated dissolved oxygen concentrations in CoL A sediments (~180 μM) were relatively lower than at CoL F (188 μM), CoL B (189 μM) and CoL C (200 μM) likely reflective of the higher intensity of respiration processes at CoL A. As mentioned above, the depth-integrated concentrations of NO_x⁻ were highest in CoL A (11.7-13.5 μM) and CoL C (10.5 μM) sediments, compared to CoL F, B, and E (4-5.9 μM) (Table 1), reflective of the differential production of NO_x⁻ below the oxygen penetration depth at each station (Figure 4). These differences were also similar in the depth-integrated Fe(II) concentrations determined by voltammetry which decreased from CoL A (95-451 μM), to CoL C (136-266 μM), CoL F (136 μM), CoL B (103 μM), and CoL E (0 μM). Depth-integrated concentrations of dissolved Fe(II) and dissolved Fe(III) quantified in the pore waters after extraction followed a slightly different pattern, likely reflective of heterogeneities in some of the sediment cores (Table 1). Although CoL A displayed the highest Fe(II) concentrations (301-476

μM), concentrations of dissolved Fe(III) at CoL A were lower (51-92 μM) than at CoL F (142 μM), which displayed relatively similar dissolved Fe(II) concentrations as at CoL A (322 μM). The iron speciation pattern in the pore waters of the other stations followed the same pattern as the electrochemical data. Dissolved Fe(II) concentrations and Fe(III) concentrations were highest in CoL C (219-249 μM Fe(II), 4-56 μM Fe(III)), followed by CoL B (109 μM Fe(II) and 26 μM Fe(III)) and CoL E (48 μM Fe(II) and undetectable Fe(III)). These findings suggest that iron reduction was equally active in CoL F and A sediments, despite the much lower NO_x^- in CoL F. As iron reduction consumes protons, the pH data seemingly corroborated the high intensity of iron reduction at these stations, as a higher average pH was found at CoL A (7.56-7.99) and CoL F (7.59) than at CoL C (7.26-7.6) and CoL B (7.33) (Table 1). Interestingly, the depth-integrated concentrations of DIC followed a different pattern between stations (Table 1). Although CoL F displayed the highest DIC (7.5 mM) of all the stations, depth-integrated DIC was also equally high at CoL C (4.3-7.6 mM) and relatively close at CoL B (5.8 mM), two stations where iron reduction was seemingly lower in intensity than at CoL A which displayed relatively lower DIC concentrations (2.7 – 4.9 mM). Depth-integrated concentrations of dissolved orthophosphates were also higher at CoL F (16 μM) and CoL B (33 μM) compared to CoL C (0.3-1.4 μM) and CoL A (1.3-4.5 μM) (Table 1). The low orthophosphate concentrations in CoL A and CoL C are likely due to their adsorption to iron oxides, as the amorphous iron oxide content was high in these sediments (60-90% of total reaction iron oxides) compared to CoL B and CoL F (Table 1). Only a single depth profile of ammonium concentrations was obtained in one of the sediment of CoL A (MTB-2). The slope of the DIC versus NH_4^+ concentrations was used to show that the

C:N ratio were about 15.2 ($R^2=0.961$) (Figure 5), a value close to the 550:30 ratio obtained from solid phase analyses.

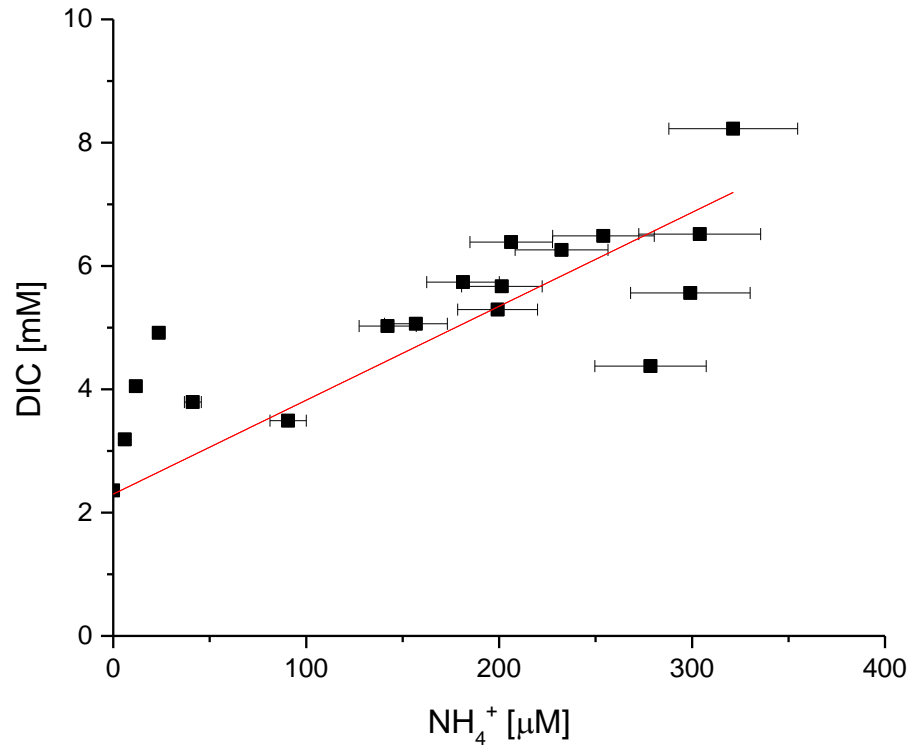


Figure 5: DIC as a function of dissolved ammonium concentrations observed at CoL A. The red line represents a C:N ratio of 15.2 with a bottom water concentration of 2.3 mM DIC ($R^2=0.961$).

Table 1: Depth Integrated Concentrations (mol/L) of Dissolved O₂, NO_x⁻, DIC, Fe(II), Fe(III), and ΣPO₄³⁻, Average pH, and Relative Ratio of Ascorbate/Dithionite-Extractable Iron Oxides (A/D) in Sediment from CoL A, CoL B, CoL C, CoL F, and CoL E. The Speciation of Iron Was Measured Both Electrochemically (EC) and in the Pore Waters After Extraction (PW). The pH Represents the Average pH Measured Electrochemically in Each Sediment Core. Ascorbate and Dithionite Iron Were Measured in the Same Sediment After Pore Water Extractions. (ND=not determined.) (*NO_x⁻ is From MTB-6 as it was not Measured in MTB-9 and Both MTB-9 and MTB-6 Were From the Same Location).

Station	O ₂ (uM)	NO _x ⁻ (uM)	Fe(II) EC (uM)	Avg. pH	DIC (mM)	Fe(II) PW (uM)	Fe(III) PW (uM)	ΣPO ₄ ³⁻ (uM)	Fe _{asc.} (μmol gdw ⁻¹)	Fe _{dit} (μmol gdw ⁻¹)	A/D (%)
A MTB-2	162.6±4.2	13.5	451.4±19.9	7.56±0.2	4.7±0.5	432.8±47.9	92.0±42.6	1.3±0.1	113.8±18.0	139.6±73.4	81.5±3.9
A MTB-13	202.5±6.0	12.0	320.8±10.9	7.99±0.3	2.7±0.4	476.0±73.2	51.1±33.9	4.5±0.8	37.9±6.8	59.2±19.4	62.6±4.2
A MTB-3	173.5±4.6	11.7	95.2±4.7	7.60±0.2	4.9±0.5	301.0±31.5	52.5±7.5	2.6±0.6	106.2±14.8	169.6±31.2	59.2±6.2
B MTB-12	175.3±0.8	4.0	103.9±18.3	7.33±0.2	5.8±0.7	108.5±12.0	25.8±5.0	33.4±5	86.6±16.7	119.1±54.3	72.8±10.3
C MTB-6	199.3±3.4	10.5	266.3±25.9	7.26±0.2	4.3±0.5	219.4±24.1	55.6±9.1	1.4±0.1	97.5±12.9	130.5±32.5	74.7±5.2
C MTB-9	174.2±2.2	10.5*	136.6±19.4	7.60±0.2	7.6±0.8	249.7±27.3	4.1±9.6	0.3±0.1	ND	ND	ND
F MTB-5	188±11.5	4.2	136.5±9.4	7.59±0.3	7.5±0.8	322.9±33.6	143±11.2	16±1.3	154.4±21.6	221.3±33.2	69.8±3.2
E MTB-14	107.9±5.0	5.9	0.00	7.96±0.1	3.5±0.4	48.3±5.3	ND	8.7±0.6	85.4±16.7	95.2±23.6	89.7±6.1

3.2 Sediment incubations

Two sets of similar incubations were conducted to determine whether the production of nitrite or nitrate could be stimulated in anoxic conditions and to examine the effect of ammonium concentrations on their production. As the results from both sets of incubations were similar (though shorter in the first set), only the second set is described here. Results of the first set can be found in the Appendix (Section B and Figure B1). The incubations revealed the simultaneous production of total Fe(II) and nitrate, but not nitrite, in all treatments (Figure 6). Similar total Fe(II) concentrations were found initially in the sediment of all treatments, ranging from 270 μM in the treatment amended with 200 μM NH_4^+ (Figure 6e) to 900 μM in the treatment amended with 10 μM NH_4^+ (Figure 6b). These relatively high initial concentrations indicate that anaerobic conditions were easily preserved in these sediments. Control incubations with Fe(II) spikes in sediment-free artificial seawater in otherwise identical reactors and conditions indicated that at most 30% of Fe(II) was lost over the course of the incubations. In the unamended treatment, total Fe(II) concentrations increased from 600 μM to 8.4 mM over 39 days, then decreased to 4.5 mM after 202 days. Total Fe(II) concentrations followed the same pattern in all NH_4^+ -amended incubations, with maximum concentrations at 39 days ranging between 8 and 10 mM in the treatments amended with 50, 100, 200, 500, and 2000 μM (Figure 6c-f and g) and up to 13 mM in the treatments amended with 10 and 1000 μM NH_4^+ (Figure 6b and g). After 202 days, total Fe(II) concentrations in all incubations were much lower, but remained high compared to the starting Fe(II) concentration, from a minimum of 2.5 mM

in the 1000 μM NH_4^+ amendment (Figure 6g) to a maximum of 5.1 mM in the 500 μM NH_4^+ amendment (Figure 6f). The sediments retained their initial deep brown color during the course of the incubations, and no sulfide odor was detected at the end of the experiments.

Ammonium concentrations in the unamended treatment increased from 135 μM to 400 μM at 20 days, then decreased to 120 μM at 85 days before increasing to 230 μM at 202 days (Figure 6a). Ammonium increased over the first 20 days in all incubations, ranging from a 70 μM increase (+50, Figure 6c) to a 1500 μM increase (+2000, Figure 6h). Between 20 and 85 days, ammonium decreased by 64-70% in the treatments amended with ≤ 50 μM NH_4^+ (Figure 6a-c), decreased by 17-33% in the treatments amended with 200, 1000, and 2000 μM NH_4^+ , and increased by 29 and 55 % in the treatments amended with 500 and 100 μM NH_4^+ . Between 85 and 202 days, a 91-268% increase in NH_4^+ concentrations was observed in the unamended, +10, and +50 μM NH_4^+ treatments. A 30-60 % increase was observed in the same time period with the +200, +500, +1000, and +2000 NH_4^+ amendments (Figure 6e-h). The 100 μM NH_4^+ treatment was the only one to decrease by 27% during the same time period (Figure 6d). Final ammonium concentrations ranged between 230 μM in the unamended control to 4.1 mM in the 2000 μM NH_4^+ amendment. Although nitrite was never detected in significant concentrations, nitrate was initially produced in the first part of all incubations, then ultimately consumed. In the unamended treatment, nitrate increased sporadically from 20 μM initially to around 36 μM at 85 days, then decreased to 8 μM at 202 days (Figure 6a). The increase in nitrate was equally sporadic during the first 40 days of the incubations of most treatments (Figure 6b, c, e, f, and h). Eventually, nitrate concentrations as high as 36

μM in the $10 \mu\text{M NH}_4^+$ amendment (Figure 6b), $50 \mu\text{M}$ in the $50 \mu\text{M NH}_4^+$ amendment (Figure 6c), $57 \mu\text{M}$ in the $100 \mu\text{M NH}_4^+$ amendment (Figure 6d), $60 \mu\text{M}$ in the $200 \mu\text{M NH}_4^+$ amendment (Figure 6e), $74 \mu\text{M}$ in the $500 \mu\text{M NH}_4^+$ amendment (Figure 6f), $62 \mu\text{M}$ in the $1000 \mu\text{M NH}_4^+$ amendment (Figure 6g), and $113 \mu\text{M}$ in the $2000 \mu\text{M NH}_4^+$ amendment (Figure 6h) were found after 85 days. Between 85 and 202 days, however, nitrate concentrations decreased in all treatments to a final concentration ranging between 8 and $10 \mu\text{M}$ in the incubations amended with less than $100 \mu\text{M NH}_4^+$ (Figure 6a-c) to between 16 and $28 \mu\text{M}$ in the incubations amended with $\geq 100 \mu\text{M NH}_4^+$ (Figure 6d-h).

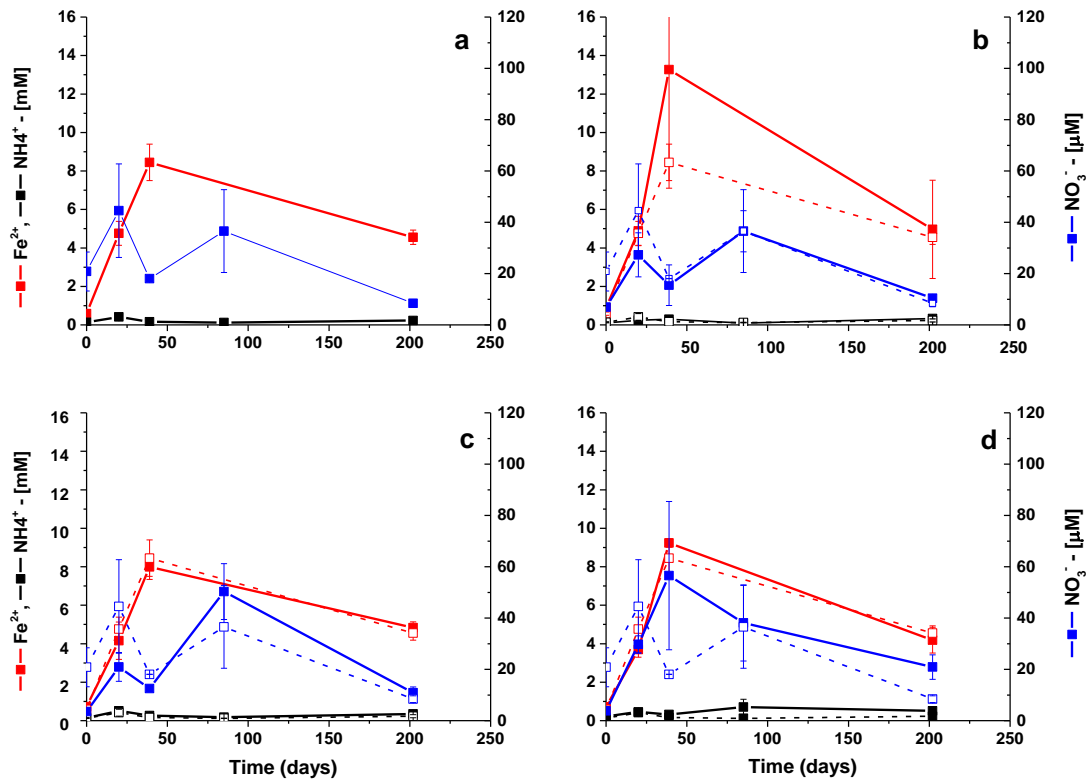


Figure 6: Fe(II), NH₄⁺, and NO₃⁻ as a function of time in sediment incubations (from CoL A bulk sediments) amended with a) 0, b) 10, c) 50, d) 100 μM NH₄⁺, e) 200, f) 500, g) 1000, and h) 2000 μM NH₄⁺. Error bars represent the standard deviation between two replicate incubations. Dashed lines in b-h represent the unamended live control to examine eventual increase in production or consumption of each species.

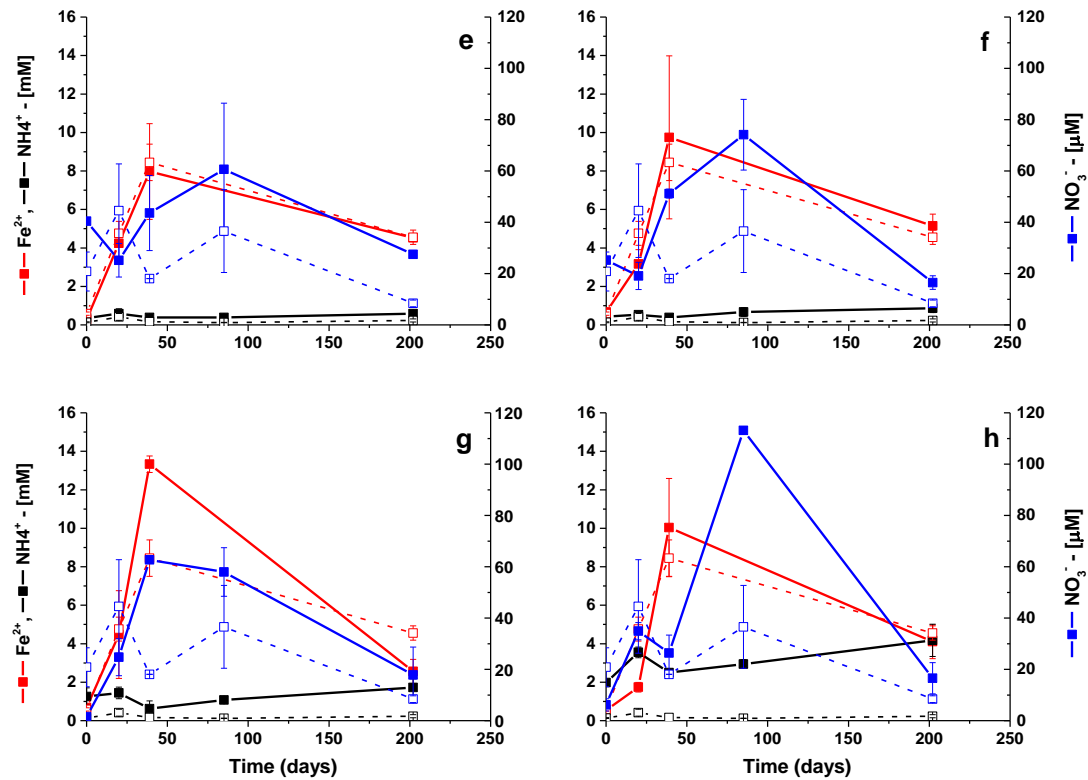


Figure 6 (cont.): Fe(II), NH₄⁺, and NO₃⁻ as a function of time in sediment incubations (from CoL A bulk sediments) amended with a) 0, b) 10, c) 50, d) 100 μM, e) 200, f) 500, g) 1000, and h) 2000 μM NH₄⁺. Error bars represent the standard deviation between two replicate incubations. Dashed lines in b-h represent the unamended control to examine eventual increase in production or consumption of each species.

CHAPTER 4: DISCUSSION

4.1 Iron reduction in Congo Lobe Sediments

Despite sulfate concentrations resembling full strength seawater, the evidence shows that the sediments from the levees and the banks along the Congo lobes are dominated by iron reduction rather than sulfate reduction. The depth-integrated Fe(II) concentrations were highest at CoL A, the entrance to the lobe complex, lower in CoL C and F, and lowest in the off-axis CoL B and the extinct channel CoL E (Table 1), suggesting that the shape of the channel influences the intensity of iron reduction. Neither dissolved sulfides (MDL < 0.2 μM) nor $\text{FeS}_{(\text{aq})}$ were detected electrochemically, both of which would be expected in carbon rich continental margin sediments, and no sulfide odor was detected during the pore water extractions and analyses. More importantly, these sediments were characterized by a deep brown color and contained high concentrations of amorphous iron oxides (300-600 $\mu\text{mole g}^{-1}_{\text{dwt}}$) and dissolved Fe(II) in the pore waters (200-700 μM). Altogether, these findings suggest that the reduction of iron oxides observed in these sediments is microbial. These findings are consistent with previous studies, as evidence for microbial iron reduction has been observed in a variety of marine environments, including coastal marsh sediments (Lowe et al., 2000; Koretsky et al. 2003; Taillefert et al., 2007), estuarine sediments (Bull and Taillefert, 2001; Meiggs and Taillefert, 2011), glacially influenced fjord sediments (Wehrmann et al., 2014), and continental margin sediments (Hyacinthe et al., 2001; van der Zee et al., 2003; Elrod et al., 2004; Severmann et al., 2006; Beckler et al., 2015). The

concentrations of iron oxides and dissolved Fe(II) reported here, however, are much higher than in most continental margin sediments. Microbial iron reduction in sediments that contain high concentrations of amorphous iron oxides should be expected, as the reduction of ferrihydrite is more thermodynamically favorable than sulfate reduction (Sørensen 1982; Beckler et al., 2015), even in seawater, at the pressure and temperature of deep-sea sediments, and in the presence of Fe(II) concentrations as high as 100 mM (Beckler et al., 2015). In contrast, when goethite is the dominant iron oxide, sulfate reduction becomes more thermodynamically favorable at Fe(II) concentrations as low as 10^{-5} M (Beckler et al., 2015). These findings explain the existence of an iron reduction zone above and below the sulfate reduction zone observed in some marine sediments (Bosselmann et al., 2003; Riedinger et al., 2014) and suggest the high concentration of ascorbate-reactive iron oxides in the Congo Lobe sediments (Table 1) creates a thermodynamic driving force that supports iron reduction, even in these deep marine sediments.

4.2 Anaerobic Nitrification in the Congo Lobe sediments

The existence of nitrate and/or nitrite (NO_x^-) subsurface peaks below the maximum oxygen penetration depth and in much higher concentrations than in the overlying waters represents a striking feature of these sediments. The production of nitrate and/or nitrite is unlikely to be attributable to canonical nitrification, which requires dissolved oxygen (Froelich et al., 1979; Costa et al., 2006), as a 1 cm gap was observed between maximum oxygen penetration (< 1 cm) and the onset of nitrate production (2 cm) in several sediment cores (Figure 4). In addition, NO_x^- decreased immediately below the aerobic zone, as would be expected from canonical denitrification (Figure 4). Finally,

nitrate accumulation in the vacuoles of some microorganisms such as *Thiomargarita*, *Thioploca*, and some *Beggiatoa* relatives (Fossing et al., 1995; Schulz et al., 1999) that could have been released by cell lysis during the centrifugation process could explain the subsurface peak in nitrate. However, these microorganisms are mainly sulfide oxidizers and the centrifugation procedure adopted in the present study does not release nitrate from such cells (Sayama, 2001). Also, such an artifact would be expected across all depth intervals, as these organisms are typically found in the top 10 cm of the sediment column. These considerations suggest that a different process is responsible for the production of NO_x^- in these sediments. Similar evidence for anaerobic nitrification has been observed in other studies and attributed to the reduction of Mn(IV) oxides coupled to ammonium oxidation (Luther et al., 1997; Hulth et al., 1999; Javanaud et al., 2011; Lin and Taillefert, 2014). Mn(II), however, was not detected in any of the CoL A sediment cores and was only detected in one core from CoL C below the onset of iron reduction and nitrate production, such that manganese reduction was likely not an important process in most of the CoL sediments. In contrast, iron reduction was demonstrated at the same depth interval as the onset of the anaerobic production of nitrate in all of the sediment cores from CoL A, CoL C, CoL F, and in a lesser extent CoL B (Figure 4), and depth-integrated concentrations of Fe(II) and NO_x^- in the MTB cores (Table 1) confirm the link between Fe(III) reduction and anaerobic nitrification. A positive correlation ($R^2=0.73$) between the overall concentrations of the product of both reactions is found in most of the cores, with the notable exception of the sediment from CoL F which shows excess Fe(II) produced compared to NO_x^- (Figure 7). As this sediment is at the entry of the youngest lobe complex, in contrast to Stations A and C (Figure 2), it is possible that

NO_x^- is more rapidly consumed than produced or, alternately, that the microbial reduction of iron oxides is more intense as suggested by the high concentrations of DIC and orthophosphates at this site relative to the others (Table 1).

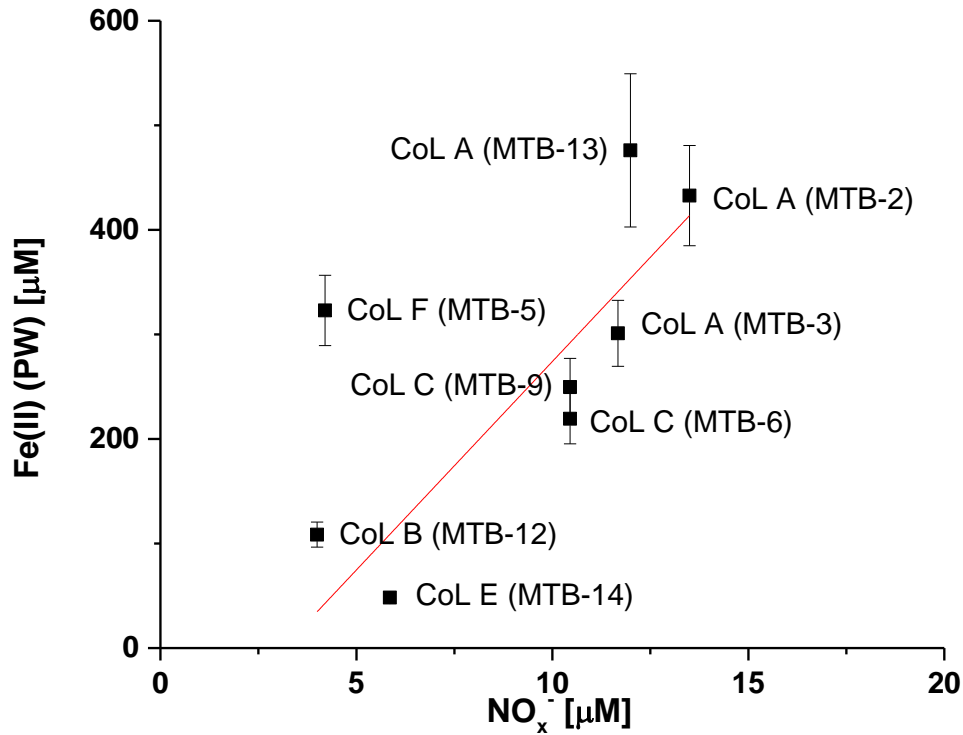


Figure 7: Correlation between depth-integrated dissolved Fe(II) and NO_x^- in the sediment cores of the Congo lobe. In general, a positive correlation ($R^2 = 0.73$) is found between the depth-integrated concentrations of Fe(II) and NO_x^- at each station, excluding CoL F.

4.3 Thermodynamics of Feammox

As the sediments are rich in iron and given evidence that microbial iron reduction can be more thermodynamically favorable in some marine environments (Beckler et al., 2015), iron reduction could plausibly be connected to anaerobic nitrification. This

process has been reported before in wastewater treatment sludge and forest soils (Park et al., 2009; Yang et al., 2012; Clément et al., 2005) even though it is not thermodynamically favorable at circumneutral pH (Thamdrup, 2012). At first glance, thermodynamic calculations for the Congo Lobe sediment (Table 2) confirm that nitrification coupled to iron reduction is not thermodynamically favorable in these conditions ($\Delta G = +146.59$ kJ/mole) and therefore the reaction should not naturally proceed. Microorganisms, however, have been known to circumvent this issue using processes such as electron bifurcation. For example, the initial step of aerobic nitrification which oxidizes ammonia to hydroxylamine by oxygen using ammonia monooxygenase (AMO) is thermodynamically not favorable unless the oxygen is activated to a more reactive form (Costa et al., 2006; Luther, 2010). To activate the oxygen molecule, two of the four electrons produced during the oxidation of hydroxylamine to nitrite are diverted back to the metal center of the AMO instead of ATP production (Costa et al., 2006). Electron bifurcation is also proposed to drive the proton motive force in several processes that would not otherwise be thermodynamically favorable. For example, the anaerobic oxidation of methane coupled to sulfate reduction, while thermodynamically favorable overall (Dale et al., 2006), requires that the anaerobic oxidation of methane be coupled to H_2 evolution which has a ΔG^0 of +135.6 kJ/mol, comparable to that calculated for iron reduction coupled to ammonium oxidation to nitrate (Table 2). The reaction only becomes thermodynamically favorable when coupled with sulfate reduction performed by a different organism, creating a symbiotic relationship (Dale et al., 2006). Another proposed pathway for this process, which still includes intermediate reactions with a positive ΔG , involves sulfate reduction to

elemental sulfur in a single organism, which is then disproportionated to sulfide and sulfate to overcome the thermodynamic barrier (Milucka et al., 2012). Other examples include the proposed anaerobic oxidation of methane coupled to nitrite reduction (Ettwig et al., 2010) and the oxidation of acetate by perchlorate reducing bacteria (Coates and Achenbach, 2004), which are both dependent on the thermodynamically unfavorable first steps of methane oxidation to methanol and perchlorate oxidation to chlorate. To circumvent these issues, electrons are again bifurcated from the proton motive force-driven electron transport chain to generate oxidants of ammonium, methane, and perchlorate. Hence, the intracellular transformation of nitric oxide to molecular oxygen, a thermodynamically favored but kinetically limited reaction, is apparently required to oxidize methane to methanol during anaerobic methane oxidation coupled to nitrate reduction (Ettwig et al., 2010). Similarly, the intracellular dismutation of chlorite into chloride and molecular oxygen in perchlorate reducing bacteria has been proposed to reduce perchlorate (Coates and Achenbach, 2004). These examples show that microbes can carry out dissimilatory processes and circumvent thermodynamic or kinetic limitations. Similarly, in the coupling of iron reduction to ammonium oxidation, the likely limiting step is the transformation of ammonium to hydroxylamine (NH_2OH) or nitric oxide (NO). Examination of the single- or two-electron transfer steps shows that iron reduction coupled to ammonium oxidation to hydroxylamine is not thermodynamically favorable at any pH, but iron reduction coupled to hydroxylamine oxidation to N_2O is favorable at $\text{pH} < 10$ (Luther, 2010). It is therefore possible that some enzymatically-produced intermediate may make this reaction thermodynamically favorable.

Table 2: Coupling of Iron Reduction to Ammonium or Nitrite Oxidation and ΔG_r Calculations in the Conditions of the Congo Lobe CoL A Sediments. The following conditions were used: pH = 7.4, $[Fe^{2+}] = 1 \mu M$, $[NO_3^-] = 1 \mu M$, $[NO_2^-] = 1 \mu M$, $[NH_4^+] = 100 \mu M$, $pN_2 = 0.718 \text{ atm}$, $pN_2O = 1E-9 \text{ atm}$

Iron reduction reactions	ΔG_r (kJ/mol)
$6 Fe(OH)_3 + 2 NH_4^+ + 10H^+ \rightarrow 6 Fe^{2+} + N_2 + 18 H_2O$	-206.90
$8 Fe(OH)_3 + 2 NH_4^+ + 14H^+ \rightarrow 8 Fe^{2+} + N_2O + 23 H_2O$	15.40
$2 Fe(OH)_3 + NO_2^- + 4H^+ \rightarrow 2Fe^{2+} + NO_3^- + 5H_2O$	47.55
$5Fe(OH)_3 + NH_4^+ + 9H^+ \rightarrow 5Fe^{2+} + NO + 14H_2O$	92.67
$6Fe(OH)_3 + NH_4^+ + 10H^+ \rightarrow 6 Fe^{2+} + NO_2^- + 16 H_2O$	99.05
$8Fe(OH)_3 + NH_4^+ + 14H^+ \rightarrow 8 Fe^{2+} + NO_3^- + 21 H_2O$	146.59

4.4 Evidence for Anaerobic Nitrification from Sediment Incubations

The sediment incubations displayed a significant accumulation of nitrate, up to 113 μM depending on the treatment (Figure 6). Simultaneously, Fe(II) accumulated to millimolar concentrations over the first 39 days in all treatments, suggesting that heterotrophic iron reduction was active in these incubations. As dissolved oxygen would have prevented the accumulation of Fe(II), these findings demonstrate that anaerobic conditions were maintained in all treatments. Indeed, sediment-free controls amended with Fe(II) showed little change in Fe(II) concentration and remained clear over 100 days, suggesting that oxygen was not leaking into the reactors. As oxygen contaminations during the incubations were not an issue, aerobic nitrification was likely not ongoing in these incubations. Moreover, as the samples collected during the incubations were not centrifuged, the release of nitrate from vacuoles of some

microorganisms such as *Thiomargarita*, *Thioploca*, and *Beggiatoa* was not responsible for the production of nitrate over time. Finally, as manganese concentrations were not significant in the sediments of the Congo Lobes, the anaerobic production of nitrate detected in the incubations over time can only be attributed to the Fe(III)-dependent oxidation of ammonium.

Using the rate of nitrate production as a function of ammonium added, it is possible to calculate the rate of Feammox following Michaelis-Menten kinetics. Given that the solid phase iron oxide content of these sediments is 200-300 $\mu\text{mol/g}$ dry wt., or 0.5 mol/L, it can be assumed that it is in excess and the rate law for Feammox is zero order with respect to iron oxides. As a result, the rate law for nitrate production by the Feammox process can be simplified to Equation 3,

$$\frac{dNO_3}{dt} = \frac{R_{max} * [NH_4^+]}{K_m + [NH_4^+]} \quad \text{Eq. 3}$$

and the R_{max} and K_m terms can be calculated using a Lineweaver-Burk plot (Figure 8).

Using this approach, a R_{max} of 0.84 (± 0.16) $\mu\text{mol/L/day}$ and a K_m of 19.1 (± 6.23) $\mu\text{mol/L}$ were determined in these incubations. Although the maximum rate of anaerobic nitrification calculated from the incubations is relatively low, the Michaelis-Menten rate constant is also low, indicating that the binding of the enzyme to the substrate is efficient. These findings suggest that the iron-dependent anaerobic oxidation of ammonium to nitrate is able to compete with heterotrophic iron reduction, despite the significant role of iron oxides in the process (8 moles required). The low maximum rate

could also indicate that the product of the anaerobic oxidation of ammonium may be removed by alternative processes (e.g. denitrification, anammox).

To examine the contribution of Feammox to Fe(II) production in the incubations, an overall rate law for Fe(II) production that includes the amount of iron that would be produced by Feammox can be determined using the overall stoichiometric coefficient of 8 moles of Fe(OH)₃ reduced for each mole of NH₄⁺ oxidized to nitrate (Equation 4).

$$\frac{dFe(II)_t}{dt} = -8 * \frac{R_{max} * [NH_4^+]}{K_m + [NH_4^+]} + R_{resp} \quad \text{Eq. 4}$$

In this rate law, R_{resp} is the rate of heterotrophic iron reduction, $[NH_4^+]$ represents the concentration of ammonium added and $\frac{dFe(II)_t}{dt}$ represents the average rate of total Fe(II) production observed in each treatment. From this relationship, the contribution of Feammox to the rate of Fe(II) production can be calculated as a function of the ammonium added (Figure 9). These calculations reveal that the maximum rate of iron reduction due to Feammox is 7.96 $\mu\text{M}/\text{day}$, which represents at most 4% of the total rate of Fe(II) production. As Feammox only contributes to a small fraction of Fe(II) production, it does not affect the iron cycle, despite the fact that 8 moles of Fe(II) are produced per mole of NH₄⁺ oxidized by Feammox.

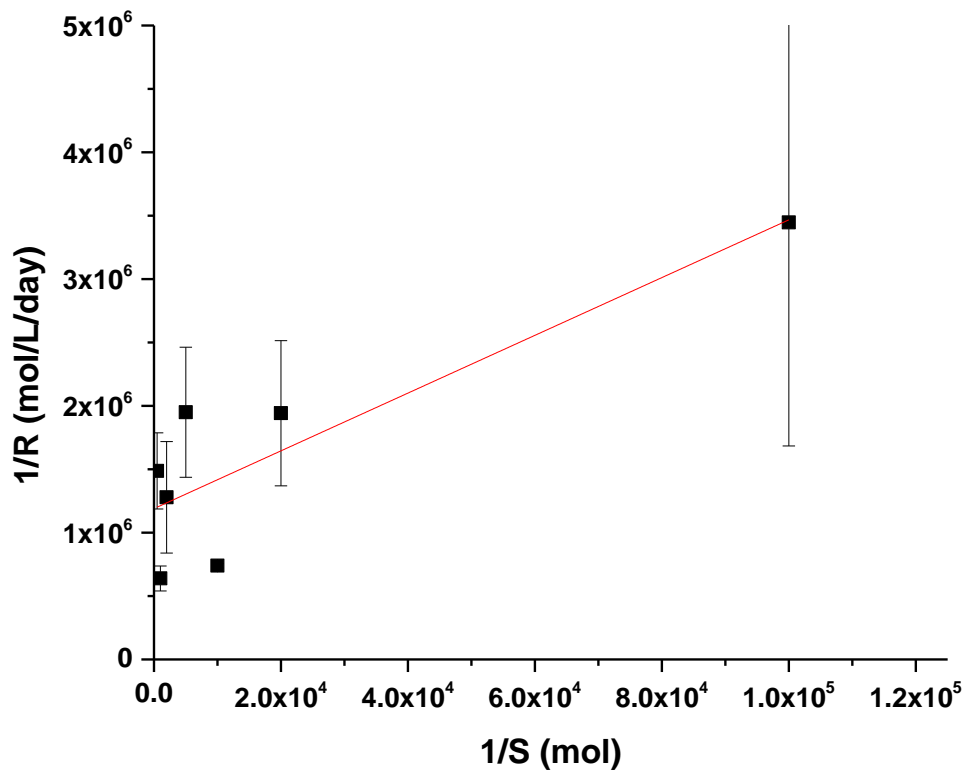


Figure 8: Lineweaver-Burk Plot for nitrate production rates (mol/L/day) as a function of moles of NH_4^+ added. R_{max} and K_m were derived using linear regression ($R^2=0.69$). Error bars represent the standard deviation of the rates.

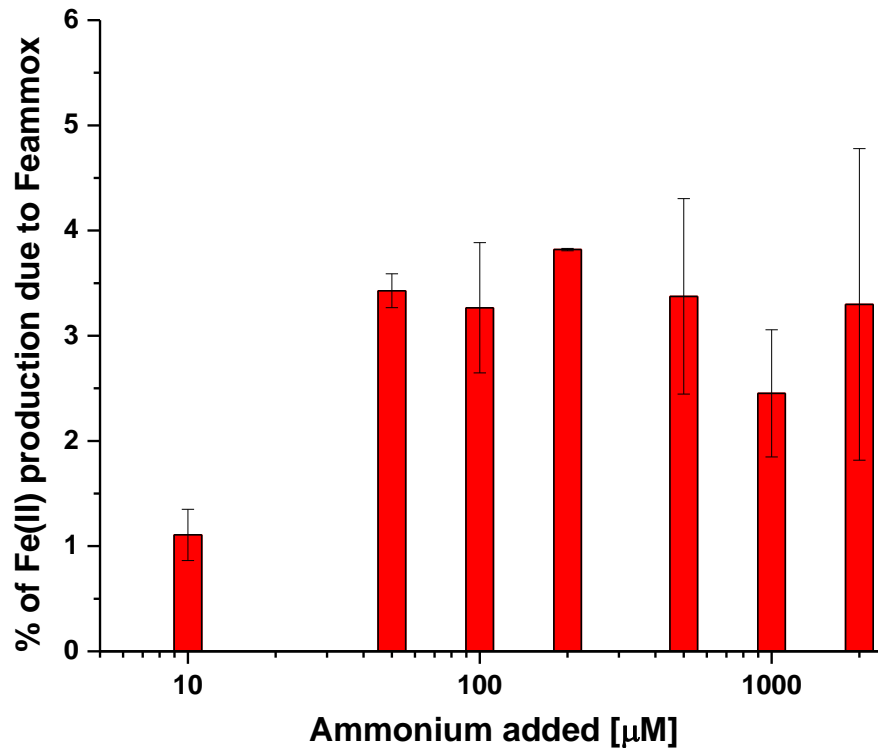
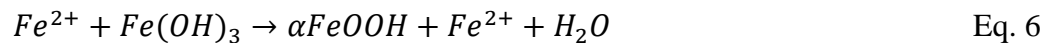
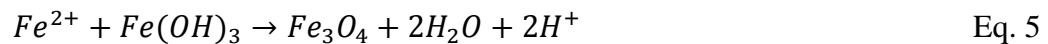


Figure 9: Percent of Fe(II) production due to Feammox in the sediment incubations as a function of ammonium added.

4.5 Evidence for Anaerobic Fe(II) Oxidation in the Sediment incubations

Total Fe(II) eventually decreased after 39 days in all treatments, but remained in the 3-4.5 mM range by the end of the incubations (Figure 6). As total Fe(II) measurements include any FeS or carbonate minerals that may have precipitated during the incubations, four different processes could explain the decrease in total Fe(II) over time: First, Fe(II) could have precipitated under the form of pyrite which is known to resist acid extractions (Kostka and Luther, 1994; Poulton and Canfield, 2005). The formation of pyrite, however, is unlikely given that pyrite requires FeS and H₂S

precursors (Rickard and Luther, 1997) and that no dissolved sulfides, sulfidic odor, or black precipitate was observed in these incubations. Second, Fe(II) could have been oxidized by amorphous iron oxides to precipitate secondary minerals such as goethite and magnetite (Hansel et al., 2005; Pedersen et al., 2005) in a process that is catalyzed by iron-reducing microorganisms (Zachara et al., 2002) and may be significant in marine sediments (Wu et al., 2011). The presence of both crystallized and amorphous iron oxides in the sediments of the Congo Lobes (Figure 3, Table 1) suggests that it may be significant. It is important to note, however, that only the secondary mineralization process resulting in the formation of magnetite (Equation 5) generates a net removal of Fe(II) from solution, as the formation of goethite merely exchanges a Fe(II) for another (Hansel et al., 2005; Pedersen et al., 2005):



As high sulfate concentrations are known to increase the relative formation of magnetite compared to goethite (Hansel et al., 2005), and as the sediment color never really changed during the course of the incubations, it is less likely that the secondary mineralization of iron oxides may have been responsible for the removal of Fe(II) in these experiments. Third, the nitrate-dependent chemolithotrophic oxidation of Fe(II) could have contributed to the removal of Fe(II), as the nitrate content decreased between 85 and 202 days in all incubations (Figure 6). The rate of nitrate removal during this phase displayed a somewhat linear positive correlation ($R^2=0.673$) with the initial amount of ammonium added (Figure 10), suggesting that as more ammonium was added to the

incubations, more nitrate was produced and then removed. Several anaerobic processes could be responsible for nitrate removal, none of which could be differentiated in the present study. These include 1) canonical denitrification (Devol, 1991), 2) anammox (Thamdrup and Dalsgaard, 2000), 3) dissimilatory nitrate reduction to ammonium (DNRA) (Boon et al., 1986), and 4) nitrate dependent iron oxidation, either microbial or abiotic (Straub et al., 1996; Van Cleemput and Baert, 1983). This could explain both the removal of iron and nitrate. Although the organisms isolated from low temperature sediments typically grow using Fe(II) minerals (i.e. FeS, siderite) as electron donor (Schippers and Jorgensen, 2002; Edwards et al., 2003), some are able to grow on dissolved Fe(II) (Edwards et al., 2003). Considering the concentrations of Fe(II) consumed during the incubations, however, between 600 and 900 μM nitrate would have been consumed by nitrate reduction to N_2 , more than one order of magnitude higher than detected in the incubations. Finally, abiotic oxidation of Fe(II) by nitrite could have been responsible for the removal of Fe(II). Although this reaction is faster at low pH, it is estimated to be fast enough at circumneutral pH to oxidize 3.5 – 5 mM Fe(II) in a couple of days (Van Cleemput and Baert, 1983; Kampschreur et al., 2011). The observed contribution of Feammox to nitrate removal correlates with that of other studies that found that Feammox could account for N_2 loss in tropical soils, riparian wetlands, and intertidal wetlands (Clément et al., 2005; Yang et al. 2012; Huang and Jaffe, 2015; Li et al., 2015).

The oxidation of iron coupled to several reactions was shown to be thermodynamically favorable in the Congo Lobe sediments (Table 3) further supporting the hypothesis that this could account for iron and nitrate removal. Although nitrite was

not directly observed in the incubations, it was likely produced by nitrate-reducing microorganisms or as an intermediate in canonical denitrification. Whether this reaction was significant is difficult to evaluate, as it would have required the production of 1.5 to 2.5 mM nitrite in these incubations, and it is likely that a combination of both nitrate-dependent chemolithotrophic and nitrite-dependent abiotic oxidation of Fe(II) may have been involved during the second part of the experiment. In summary, although the secondary mineralization of amorphous iron oxides may have removed part of the Fe(II) produced in these incubations, it appears likely that most of the Fe(II) was oxidized either by nitrate-reducing chemolithotrophic microorganisms or abiotically by nitrite produced during the reduction of nitrate by nitrate-reducing or denitrifying microorganisms.

Table 3: Coupling of Iron Oxidation to Nitrate or Nitrite Reduction and ΔG_r Calculations in the Conditions of the Congo Lobe CoL A Sediments. The following conditions were used: pH = 7.4, $[Fe^{2+}] = 600 \mu M$, $[NO_3^-] = 100 \mu M$, $[NO_2^-] = 1 \mu M$, $[NH_4^+] = 1 \mu M$, $pN_2 = 0.718 \text{ atm}$, $pN_2O = 1E-9 \text{ atm}$.

Iron oxidation reactions	ΔG_r (kJ/mol)
$10 Fe^{2+} + 2NO_3^- + 24H_2O \rightarrow N_2 + 10Fe(OH)_3 + 18H^+$	-688.57
$6 Fe^{2+} + 2NO_2^- + 14H_2O \rightarrow N_2 + 6Fe(OH)_3 + 10H^+$	-505.53
$8 Fe^{2+} + 2NO_3^- + 19H_2O \rightarrow N_2O + 8Fe(OH)_3 + 14H^+$	-473.45
$2Fe^{2+} + NO_3^- + 5H_2O \rightarrow 2Fe(OH)_3 + NO_2^- + 4H^+$	-169.85
$4 Fe^{2+} + 2NO_2^- + 9H_2O \rightarrow N_2O + 4Fe(OH)_3 + 6H^+$	-290.41
$5 Fe^{2+} + NO_3^- + 7H_2O \rightarrow NO + 3Fe(OH)_3 + 5H^+$	-286.30
$6Fe^{2+} + NO_2^- + 16H_2O \rightarrow 6Fe(OH)_3 + NH_4^+ + 10H^+$	-208.41
$2Fe^{2+} + 2 NO + 5H_2O \rightarrow 2Fe(OH)_3 + 2N_2O + 4H^+$	-200.95
$Fe^{2+} + NO_2^- + 2H_2O \rightarrow NO + Fe(OH)_3 + H^+$	-39.13

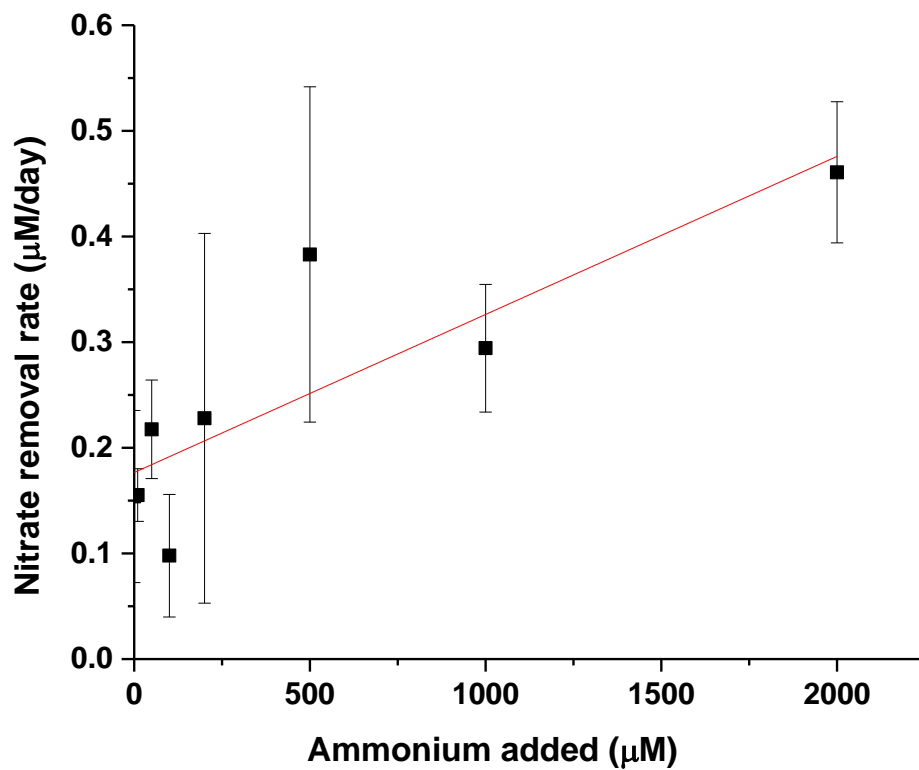


Figure 10: Net nitrate removal (uM/day) in the second phase (days 85-202) for the second incubations as a function of ammonium added. The rates display a positive linear correlation ($R^2=0.673$). Error bars represent the difference in rates between replicates.

4.6 Diagenetic modeling of the Congo Lobe sediments and Feammox

The one dimensional transient diagenetic model MATSEDLAB (Couture et al., 2010), modified to include reactions involving the nitrogen cycle (Appendix, Table A1-3) was compared at steady-state (i.e. by running the model for 200 years) to the field data from CoL A to determine whether the subsurface nitrate peaks could be reproduced using conventional aerobic nitrification, denitrification, and ammonification (Figure 11). The benthic flux of iron oxides was optimized (i.e. $70 \mu\text{mol cm}^{-2} \text{yr}^{-1}$) to match the surface concentration of iron oxides, and the Michaelis-Menten rate constant of aerobic respiration was optimized to match the dissolved oxygen profile. Finally, the intensity of aerobic nitrification and denitrification were varied systematically by changing the rate constant of aerobic nitrification and the inhibition of denitrification by dissolved oxygen. The kinetics of the other reactions remained unchanged: Abiotic Fe(II) oxidation by dissolved oxygen, siderite precipitation and dissolution, sulfate reduction, sulfidization of organic matter, $\text{FeS}_{(s)}$ precipitation and dissolution, and ammonification were fixed with rate laws and rate constants obtained from the literature (see Appendix, Table A3). In general, the diagenetic model reproduced the field data fairly well (Figure 11). The model accurately demonstrated the depletion of dissolved O_2 in the first centimeter, reflecting the intensity of aerobic respiration (Figure 11a), and the presence of oxygen in the first centimeter led to an increase in the concentration of iron oxides attributed to aerobic Fe(II) oxidation (Figure 11c). Heterotrophic iron reduction decreased the concentration of iron oxides below the depth of oxygen penetration and reproduced the increase in Fe(II) fairly well (Figure 11c). Sulfate reduction was inhibited such that neither a sulfate decrease or sulfide accumulation was observed, in agreement with the CoL A data

(Figure 11d). Although the model reproduced the dissolved O₂ profile, the increase in ammonium with depth, predicted with the C:N ratio obtained from the field data (Figure 5), and the subsurface peak in nitrate could never be reproduced (dashed lines in Figure 11b) even in the absence of denitrification (not shown). These findings confirm that another anaerobic process that oxidizes ammonium to nitrate is required to reproduce the nitrate profile. Adding the Feammox reaction helped produce nitrate in anaerobic conditions, but the high denitrification rate required to fit the data in the first 2 cm of the sediment prevented enough accumulation of nitrate below the maximum O₂ penetration depth (not shown). Decreasing the sensitivity of the denitrifying enzyme for nitrate by two folds (i.e. changing the K_m from 0.01 to 100 μmol cm⁻³) and adding anammox to the model (Reaction R13 in Table A-2 of the Appendix) using kinetic parameters within an order of magnitude from the literature (Strous et al., 1999) allowed to fit the ammonium profile and reproduce fairly well the subsurface peak in nitrate (plain line in Figure 11b). Further investigation into the effect of the rates of aerobic nitrification, denitrification, and anammox may help refine these profiles, however, in a first approximation this exercise suggests the only way to generate a subsurface peak in nitrate is to clearly separate the zones of heterotrophic denitrification and anammox by a zone of iron-dependent anaerobic nitrification. The confinement of Feammox between these two layers may potentially help future cultivation studies.

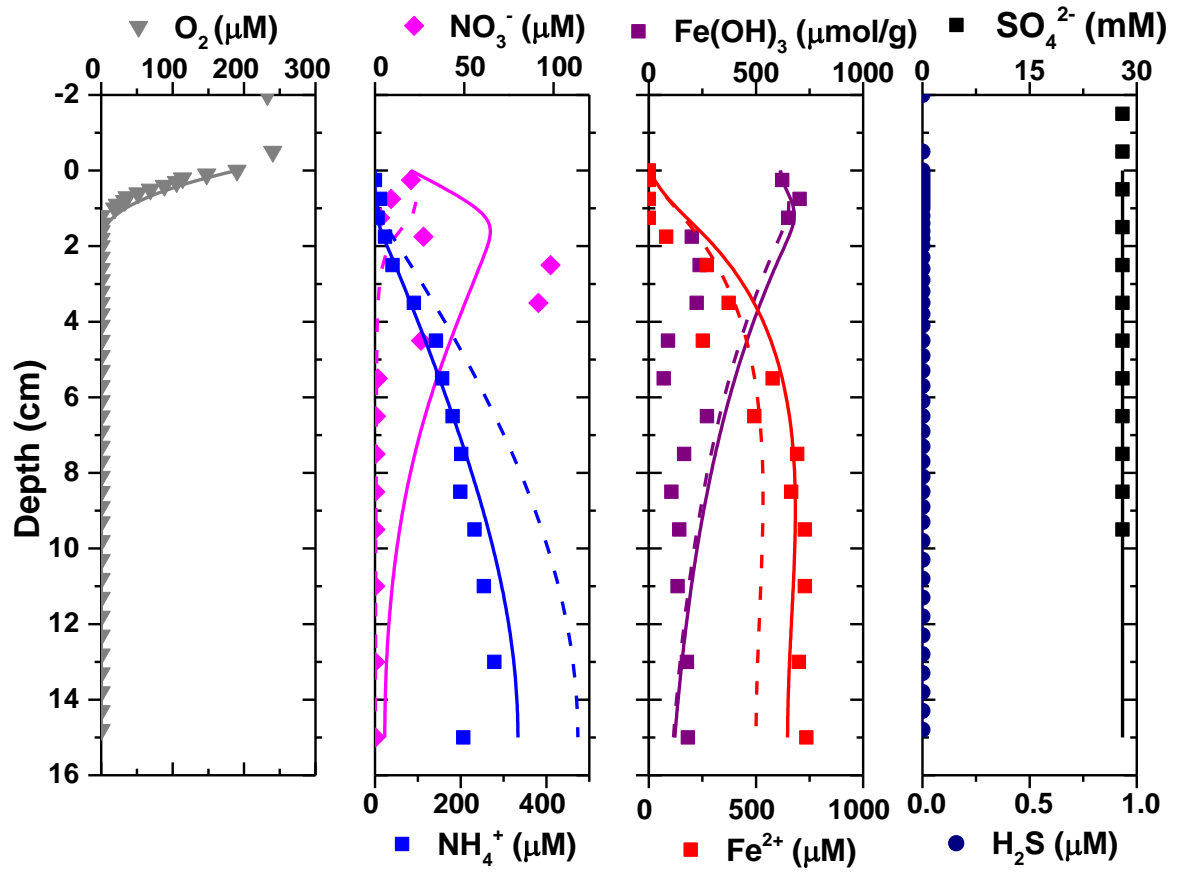


Figure 11: Comparison of the diagenetic model (lines) compared with field data from CoL A (symbols): a) O_2 (gray), b) NO_3^- (pink) and NH_4^+ (blue), c) $Fe(OH)_3$ (purple), d) SO_4^{2-} (black), ΣH_2S (blue). Dashed lines represent the results without Feammox and anammox in the model.

CHAPTER 5: CONCLUSIONS

The nitrogen cycle is essential to all life on earth, yet fixed nitrogen is scarce. Conventionally, ammonium was thought to be oxidized to nitrate solely in the presence of oxygen. The recent discovery of the anammox process, in which ammonium is oxidized anaerobically to N_2 with nitrite as an electron acceptor, provides an alternate pathway to nitrogen loss in marine sediments. Anammox, however, requires nitrite from nitrifying organisms and anammox microorganisms are strongly inhibited by dissolved oxygen, suggesting its importance may be limited to a narrow zone below the sediment-water interface. In this regard, manganese may contribute to the expansion of the anammox and heterotrophic denitrification zones by providing a source of nitrite in suboxic sediments via manganese reduction-dependent anaerobic nitrification. In continental margin sediments, however, manganese is relatively scarce raising questions regarding the importance of this process in the nitrogen cycle. The present study presents evidence that iron-dependent anaerobic nitrification can be a significant process in deep sea marine environments as well. The unique submarine canyon geology of the Congo Lobe brings organic matter and iron oxides to deep marine sediments, creating an iron-reduction dominated environment that also produces an unusual accumulation of nitrate in sediments that lack oxygen. Anaerobic batch reactor incubations of these sediments amended with ammonium demonstrated that over 100 μM nitrate could accumulate in concurrence with active iron reduction. Although heterotrophic iron reduction was responsible for over 90% of the Fe(II) production in these incubations, Feammox seems to be efficient enough to contribute to the cycling of nitrogen. A significant fraction of total Fe(II) was eventually removed in these incubations, likely due to a combination of

abiotic oxidation by nitrite, microbial nitrate or nitrite dependent iron oxidation, and secondary mineralization of Fe(II) to form magnetite. Overall, these experiments demonstrate that the iron-dependent anaerobic production of nitrate may catalyze denitrification via heterotrophic denitrification or anammox. Indeed, comparison of geochemical profiles from the Congo Lobe with a diagenetic model accounting for known heterotrophic and secondary reactions only reproduced the subsurface accumulation of nitrate when distinct zones of denitrification, Feammox, and anammox were added to the model. Future work on these sediments could include incubations that employ stable isotopes to determine the proportions of denitrification, anammox, and Feammox in these sediments. Flow-through reactor incubations could also be used to isolate the Feammox process from other nitrogen transforming reactions and enrich for these microorganisms. Future field investigations could also look for Feammox in other coastal and river-dominated continental margin sediments rich in iron oxides to better understand the global impact of this process.

APPENDIX A

Table A 1: Heterotrophic Processes in MATSEDLAB. F[species] Represents the Fraction of Natural Organic Matter Remineralized by Each Component Assuming Michaelis-Menten Kinetics. Denitrification, Iron Reduction, and Sulfate Reduction, are Inhibited by Dissolved Oxygen, Nitrate, and/or Iron Oxides According to a Non-Linear Term Function of the Concentration of Each Inhibitor and an Inhibition Constant (K^I). *accel*=acceleration factor for aerobic respiration.

Term	Description/Reaction	Model formulation
R_c	Organic matter degradation	$R_c = k_{org} * [OM]$
f_{O_2}	Aerobic respiration (R1)	$f_{O_2} = \frac{[O_2]}{K_{O_2} + [O_2]}$
f_{NO_3}	Denitrification (R2)	$f_{NO_3} = \frac{[NO_3]}{K_{NO_3} + [NO_3]} \frac{K_{O_2}^I}{K_{O_2}^I + [O_2]}$
f_{FeOH_3}	Iron reduction (R3)	$f_{FeOH_3} = \frac{[FeOH_3]}{K_{FeOH_3} + [FeOH_3]} \frac{K_{O_2}^I}{K_{O_2}^I + [O_2]} \frac{K_{NO_3}^I}{K_{NO_3}^I + [NO_3]}$
f_{SO_4}	Sulfate reduction (R4)	$f_{SO_4} = \frac{[SO_4]}{K_{SO_4} + [SO_4]} \frac{K_{O_2}^I}{K_{O_2}^I + [O_2]} \frac{K_{NO_3}^I}{K_{NO_3}^I + [NO_3]} \frac{K_{FeOH_3}^I}{K_{FeOH_3}^I + [FeOH_3]}$
R1	$(CH_2O)_x(NH_3)_y(H_3PO_4) + xO_2$ $\rightarrow xHCO_3^- + yNH_4^+ + HPO_4^{2-} + (x - y + z)H^+$	$R1 = R_c f_{O_2} accel$
R2	$(CH_2O)_x(NH_3)_y(H_3PO_4) + 0.8xNO_3^- + (-.2x + y - 2)H^+$ $\rightarrow xHCO_3^- + yNH_4^+ + HPO_4^{2-} + 0.4N_2 + 0.4H_2O$	$R11 = R_c f_{NO_3}$
R3	$(CH_2O)_x(NH_3)_y(H_3PO_4) + 4xFe(OH)_3 + (7x + y - 2)H^+$ $\rightarrow 4xFe^{2+} + xHCO_3^- + yNH_4^+ + HPO_4^{2-} + 10xH_2O$	$R2 = R_c f_{FeOH_3}$
R4	$(CH_2O)_x(NH_3)_y(H_3PO_4) + 0.5xSO_4^{2-}$ $\rightarrow 0.5xH_2S + xHCO_3^- + yNH_4^+ + HPO_4^{2-} + (2 - y)H^+$	$R3 = R_c f_{SO_4}$

Table A 2: Complete List of the Secondary Reactions Implemented in the 1D Reactive Transport Model MATSEDLAB and Their Kinetic Formulation.

Description(ID)	Reaction	Kinetic formulation
Sulfide oxidation by O ₂ (R5)	$H_2S + 2O_2 \rightarrow SO_4^{2-} + 2H^+$	$k_{tsox} [Fe(II)] [O_2]$
Iron oxidation by O ₂ (R6)	$4Fe^{2+} + O_2 + 10H_2O \rightarrow$ $4Fe(OH)_3 + 8H^+$	$k_{feox} pO_2 [Fe(II)][OH^-]^2$
H ₂ S oxidation by Fe(III) oxides (R7)	$H_2S + 2Fe(OH)_3 \rightarrow$ $2Fe^{2+} + S(0) + 6H_2O$	$k_{tsfe} [Fe(OH)_3] [\Sigma H_2S]$
FeS precipitation (R8)	$Fe^{2+} + HS^- \rightarrow FeS_s + H^+$	$k_{fepre} (\Omega_{FeS} - 1)$
FeS dissolution (R_8)	$FeS_s + H^+ \rightarrow Fe^{2+} + HS^-$	$k_{fedis} [FeS] (1 - \Omega_{FeS})$
Siderite precipitation (R9)	$Fe^{2+} + CO_3^{2-} \rightarrow FeCO_{3(s)}$	$k_{sidpre} (\Omega_{sid} - 1)$
Siderite dissolution (R_9)	$FeCO_{3(s)} \rightarrow Fe^{2+} + CO_3^{2-}$	$k_{siddis} (\Omega_{sid} - 1)$
Sulfidization of organic matter (R10)	$OM + H_2S \rightarrow OM - H_2S$	$k_{sorg} [OM][\Sigma H_2S]$
Aerobic nitrification (R11)	$NH_4^+ + 2O_2 \rightarrow NO_3^- + 2H^+ + H_2O$	$k_{nh4ox} [NH_4^+] [O_2]$
Feammox (R12)	$8Fe(OH)_3 + NH_4^+ + 14H^+ \rightarrow$ $8Fe^{2+} + NO_3^- + 21H_2O$	$\frac{[NH_4^+] R_{maxn}}{[NH_4^+] + K_{mn}}$
Anammox (R13)	$NH_4^+ + NO_2^- \rightarrow N_2 + 2H_2O$	$\frac{[NH_4^+] R_{maxnh4} [NO_3]}{K'_{NH4} + [NH_4^+] + K'_{NO3} + [NO_3]}$

Table A 3: Complete List of Constants Used in MATSEDLAB. M=fit to model data. L=literature: 1) Couture et al., 2010, 2) Wang and Van Capellen 1996,3) Millero and Schreiber 1982, 4) Stumm and Morgan, 1996, 5) Rickard, 2006, 6) Strous et al., 1999.

Name	Description	Value	Source
k_{org}	Organic matter decay constant	170 yr ⁻¹	M
K_{O_2}	K_m for aerobic respiration	0.2 $\mu\text{mol}/\text{cm}^3$	M
$accel$	R_{max} for aerobic respiration	3	M
K_{NO_3}	K_m for denitrification	0.01 $\mu\text{mol}/\text{cm}^3$	L (2)
$K_{O_2}^I$	Inhibition by O ₂	0.001 $\mu\text{mol}/\text{cm}^3$	M
K_{FeOH_3}	K_m for iron reduction	10,000 $\mu\text{mol}/\text{g}$	M
$K_{NO_3}^I$	Inhibition by nitrate	10 $\mu\text{mol}/\text{cm}^3$	M
K_{SO_4}	K_m of sulfate reduction	1.6 $\mu\text{mol}/\text{cm}^3$	M
$K_{FeOH_3}^I$	Inhibition by iron oxides	1E-6 $\mu\text{mol}/\text{cm}^3$	M
k_{tsox}	Sulfide oxidation by O ₂	1E3 cm ³ $\mu\text{mol}^{-1}\text{yr}^{-1}$	L (1)
k_{fex}	Iron oxidation by O ₂	10 ^{11.38} g ³ $\mu\text{mol}^{-3}\text{yr}^{-1}$	L (3)
k_{tsfe}	Rate constant for sulfide oxidation by iron oxides	2.5 cm ³ $\mu\text{mol}^{-1}\text{yr}^{-1}$	L (1)
K_{FeS}	Stability constant for FeS	10 ^{-0.5} $\mu\text{mol}/\text{cm}^3$	L (5)
k_{fepre}	FeS precipitation rate constant	1500 $\mu\text{mol g}^{-1}\text{yr}^{-1}$	L (1)
k_{fedis}	FeS dissolution rate constant	1E-3 yr ⁻¹	L (1)
k_{nh4ox}	Rate constant for aerobic nitrification	2E5 $\mu\text{mol}/\text{cm}^3/\text{yr}$	M
R_{maxn}	R_{max} for Feammox	0.31 $\mu\text{mol}/\text{cm}^3/\text{yr}$	This study
K_{mn}	K_m for Feammox	0.019 $\mu\text{mol}/\text{cm}^3$	This study
K_{sid}	Stability constant for FeCO ₃	10 ^{-5.03} ($\mu\text{mol}/\text{cm}^3$) ²	L (4)
k_{sidpre}	Precipitation rate constant for FeCO ₃	0.65 $\mu\text{mol g}^{-1}\text{yr}^{-1}$	L (2)
R_{maxnh4}	R_{max} for anammox	1E6 cm ³ $\mu\text{mol}^{-1}\text{yr}^{-1}$	L (6), M
K'_{NH_4}	K_m for NH ₄ ⁺ in anammox	20 $\mu\text{mol}/\text{cm}^3$	L (6), M
K'_{NO_3}	K_m for NO ₃ ⁻ in anammox	500 $\mu\text{mol}/\text{cm}^3$	L (6), M

APPENDIX B

Results of first incubations

Results of the first set of sediment incubations are presented in Figure B1. The control sediment incubations (no added ammonium) contained 2 mM total Fe(II) initially, which increased to almost 4 mM over 62 days (Figure B1a). In these incubations, ammonium rose from 101 to 218 μM over 40 days, while nitrate increased slightly (from 46 to 59 μM) after 62 days. In parallel incubations amended with increasing concentrations of ammonium, total Fe(II) decreased from 2 to 1.3 mM over 62 days (10 μM amendment, Figure B1b) or remained constant around 2.5 mM (50 and 100 μM amendment, Figure B1c-d), while ammonium remained constant at approximately 250-300 μM (Figure B1b-d). Nitrate initially decreased from about 75 to 40-50 μM depending on the ammonium amendment but then rebounded, showing no overall change (Figure B1b-d). As the concentration of ammonium was increased further in parallel incubations, total Fe(II) generally increased from 1.3 to 4.1 mM over the first 40 days in the 200 μM -amendment (Figure B1e), from 0.95 to 2.4 mM during the first 12 days in the 500 μM amendment (Figure B1f), and from 1.7 to 3.8 mM during the first 40 days in the 1000 μM amendment (Figure B1g). Its concentration then decreased to approximately 1.8 mM after 65 days in each of these treatments (Figure B1e-g). In contrast, Fe(II) remained constant near 2.1 mM in the incubations amended with the highest ammonium concentration (Figure B1h). In the same incubations, ammonium increased slightly from

485 to 625 μM over 40 days (Figure B1e) while it either decreased from 1.4 to 1.1 mM (Figure B1f) or remained constant in the treatments with higher initial ammonium concentration (Figure B1g-h). In turn, nitrate remained between 60 and 80 μM throughout the incubations amended with 200 μM ammonium (Figure B1e), decreased from 140 to 87 μM in the 500 μM amendment, decreased steadily from 120 μM initially to 65 μM after 62 days in the incubations amended with 1000 μM ammonium (Figure B1g), and increased from 45 μM initially to 68 μM over 62 days in the incubations amended with 2000 μM ammonium (Figure B1h).

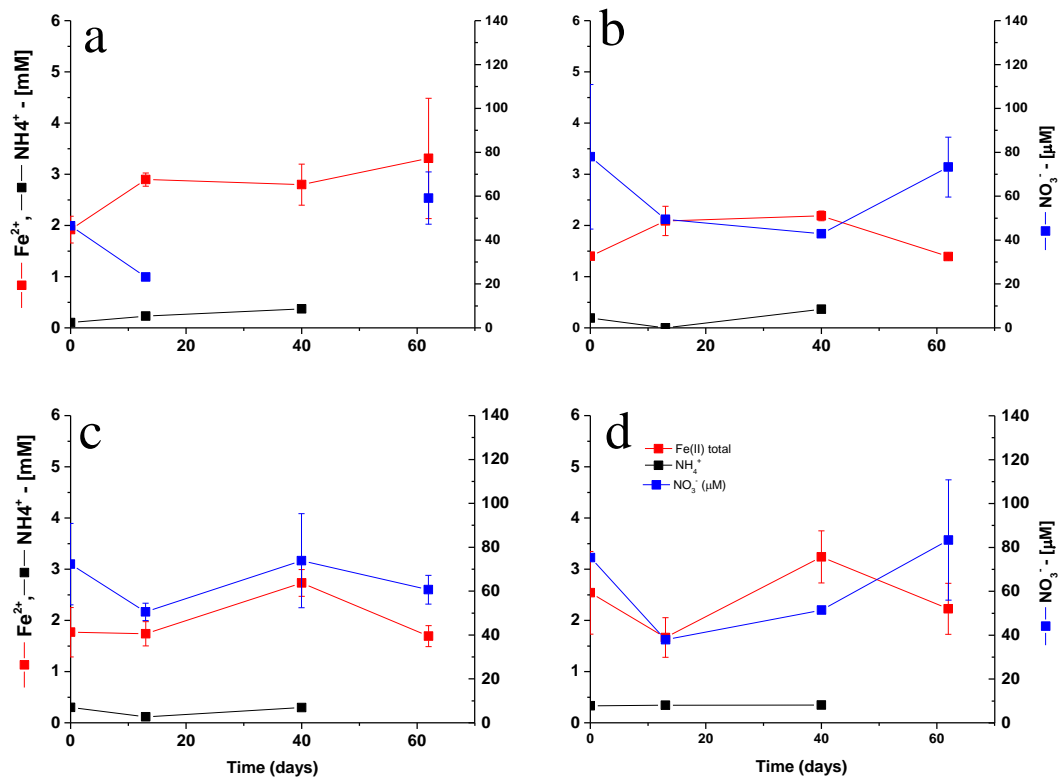


Figure B 1: Fe(II), NH₄⁺, and NO₃⁻ as a function of time in the first set of sediment incubations (from CoL A bulk sediments) amended with a) 0, b) 10, c) 50, d) 100 μM, e) 200, f) 500, g) 1000, and h) 2000 μM NH₄⁺. Error bars represent the standard deviation between two replicate incubations.

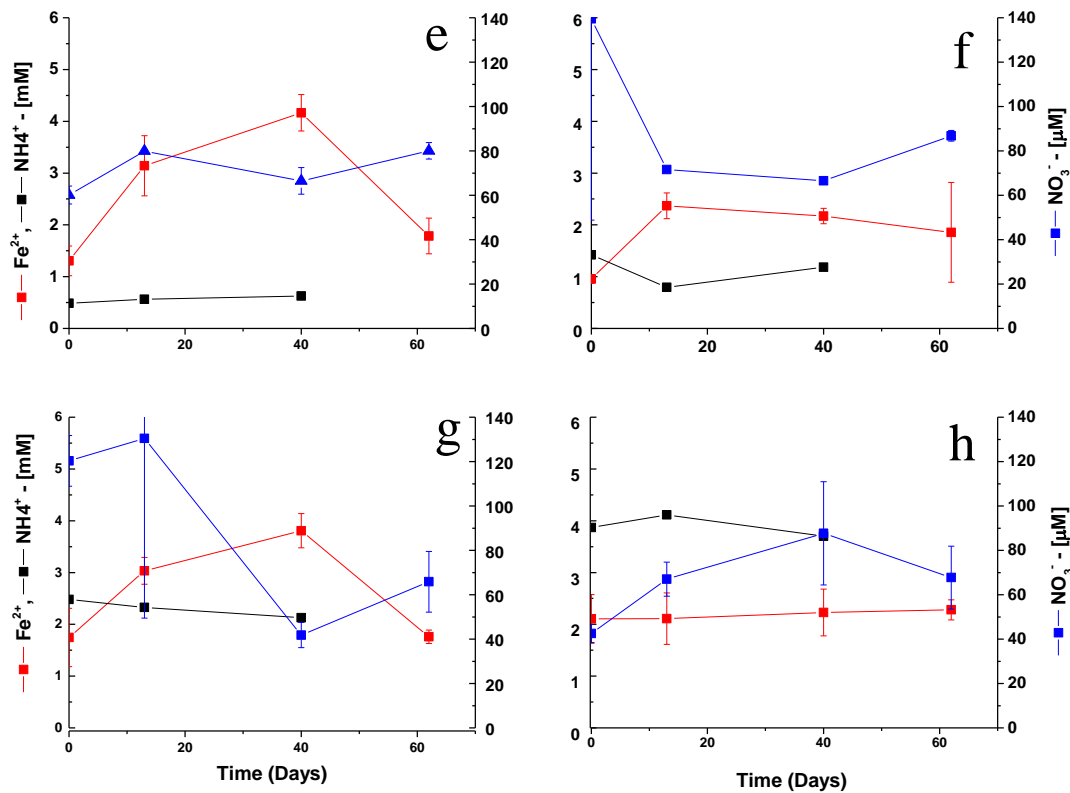


Figure B1 (cont.): Results from the first set of incubations. $\text{Fe}(\text{II})$, NH_4^+ , and NO_3^- as a function of time in sediment incubations (from CoL A bulk sediments) amended with a) 0, b) 10, c) 50, d) 100 μM , e) 200, f) 500, g) 1000, and h) 2000 μM NH_4^+ . Error bars represent the standard deviation between two replicate incubations.

REFERENCES

- Aller, Robert C., Christina Heilbrun, Caterina Panzeca, Zhongbin Zhu, and Frédéric Baltzer. "Coupling between Sedimentary Dynamics, Early Diagenetic Processes, and Biogeochemical Cycling in the Amazon–Guianas Mobile Mud Belt: Coastal French Guiana." *Marine Geology* 208, no. 2–4 (2004): 331-360.
- An, Soonmo, and Wayne S Gardner. "Dissimilatory Nitrate Reduction to Ammonium (Dnra) as a Nitrogen Link, Versus Denitrification as a Sink in a Shallow Estuary (Laguna Madre/Baffin Bay, Texas)." *Marine Ecology Progress Series* 237, no. 4 (2002).
- Anschutz, Pierre, Karine Dedieu, Franck Desmazes, and Gwénaëlle Chaillou. "Speciation, Oxidation State, and Reactivity of Particulate Manganese in Marine Sediments." *Chemical Geology* 218, no. 3–4 (2005): 265-279.
- Babonneau, N., B. Savoye, M. Cremer, and B. Klein. "Morphology and Architecture of the Present Canyon and Channel System of the Zaire Deep-Sea Fan." *Marine and Petroleum Geology* 19, no. 4 (2002): 445-467.
- Bartlett, Rebecca, Robert J. G. Mortimer, and Katherine Morris. "Anoxic Nitrification: Evidence from Humber Estuary Sediments (Uk)." *Chemical Geology* 250, no. 1-4 (2008): 29-39.
- Beckler, Jordon, Nicole Kiriazis, C. Rabouille, Frank Stewart, and Martial Taillefert. "Importance of Microbial Iron Reduction in Deep Sediments of River-Dominated Continental-Margins." In *Marine Chemistry*, 2015.
- Blodau, C., S. Hoffmann, A. Peine, and S. Peiffer. "Iron and Sulfate Reduction in the Sediments of Acidic Mine Lake 116 (Brandenburg, Germany): Rates and Geochemical Evaluation." *Water, Air, and Soil Pollution* 108, no. 3-4 (1998): 249-270.
- Boon, P. L., D. J. W. Moriarty, and P. G. Saffigna. "Nitrate Metabolism in Sediments from Seagrass (*Zostera Capricorni*) Beds of Moreton Bay, Australia." *Marine Biology* 91, no. 2 (1986): 269-275.
- Bosselmann, K, ME Böttcher, M Billerbeck, E Walpersdorf, A Theune, D De Beer, M Hüttel, HJ Brumsack, and BB Jørgensen. "Iron-Sulfur-Manganese Dynamics in Intertidal Surface Sediments of the North Sea." *Ber. Forschungsz. Terramare* 12, (2003): 32-35.
- Brandes, Jay A., Allan H. Devol, and Curtis Deutsch. "New Developments in the Marine Nitrogen Cycle." *Chemical Reviews* 107, no. 2 (2007): 577-589.
- Brandtsma, Joost, Jack van de Vossenbergh, Nils Risgaard-Petersen, Markus C. Schmid, Pia Engström, Karinh Eurenus, Stefan Hulth, Andrea Jaeschke, Ben Abbas, Ellen C. Hopmans, Mark Strous, Stefan Schouten, Mike S. M. Jetten, and Jaap S. Sinninghe Damsté. "A Multi-Proxy Study of Anaerobic Ammonium Oxidation in Marine Sediments of the Gullmar Fjord, Sweden." *Environmental Microbiology Reports* 3, no. 3 (2011): 360-366.

- Brendel, Paul J., and George W. Luther, III. "Development of a Gold Amalgam Voltammetric Microelectrode for the Determination of Dissolved Fe, Mn, O₂, and S(-II) in Porewaters of Marine and Freshwater Sediments." *Environ Sci Technol* 29, no. 3 (1995): 751-761.
- Bristow, Gwendolyn, and Martial Taillefert. "Voltint: A Matlab®-Based Program for Semi-Automated Processing of Geochemical Data Acquired by Voltammetry." *Computers & Geosciences* 34, no. 2 (2008): 153-162.
- Bull, David C, and Martial Taillefert. "Seasonal and Topographic Variations in Porewaters of a Southeastern USA Salt Marsh as Revealed by Voltammetric Profiling." *Geochemical Transactions* 2, no. 1 (2001): 104-111.
- Canfield, Donald E., Alexander N. Glazer, and Paul G. Falkowski. "The Evolution and Future of Earth's Nitrogen Cycle." *Science* 330, no. 6001 (2010): 192-196.
- Clément, Jean-Christophe, Junu Shrestha, Joan G. Ehrenfeld, and Peter R. Jaffé. "Ammonium Oxidation Coupled to Dissimilatory Reduction of Iron under Anaerobic Conditions in Wetland Soils." *Soil Biology and Biochemistry* 37, no. 12 (2005): 2323-2328.
- Coates, John D., and Laurie A. Achenbach. "Microbial Perchlorate Reduction: Rocket-Fuelled Metabolism." *Nat Rev Micro* 2, no. 7 (2004): 569-580.
- Costa, E., J. Perez, and J. U. Kreft. "Why Is Metabolic Labour Divided in Nitrification?" *Trends Microbiol* 14, no. 5 (2006): 213-9.
- Couture, Raoul-Marie, Babak Shafei, Philippe Van Cappellen, André Tessier, and Charles Gobeil. "Non-Steady State Modeling of Arsenic Diagenesis in Lake Sediments." *Environ Sci Technol* 44, no. 1 (2009): 197-203.
- Dale, A. W., P. Regnier, and P. Van Cappellen. "Bioenergetic Controls on Anaerobic Oxidation of Methane (Aom) in Coastal Marine Sediments: A Theoretical Analysis." *American Journal of Science* 306, no. 4 (2006): 246-294.
- Devol, Allan H. "Direct Measurement of Nitrogen Gas Fluxes from Continental Shelf Sediments." *Nature* 349, no. 6307 (1991): 319-321.
- Ding, L. J., X. L. An, S. Li, G. L. Zhang, and Y. G. Zhu. "Nitrogen Loss through Anaerobic Ammonium Oxidation Coupled to Iron Reduction from Paddy Soils in a Chronosequence." *Environ Sci Technol* 48, no. 18 (2014): 10641-10647.
- Dupré, Bernard, Jérôme Gaillardet, Dominique Rousseau, and Claude J. Allègre. "Major and Trace Elements of River-Borne Material: The Congo Basin." *Geochimica et Cosmochimica Acta* 60, no. 8 (1996): 1301-1321.

- Edwards, K. J., D. R. Rogers, C. O. Wirsen, and T. M. McCollom. "Isolation and Characterization of Novel Psychrophilic, Neutrophilic, Fe-Oxidizing, Chemolithoautotrophic α - and γ -Proteobacteria from the Deep Sea." *Appl Environ Microbiol* 69, no. 5 (2003): 2906-2913.
- Elrod, Virginia A., William M. Berelson, Kenneth H. Coale, and Kenneth S. Johnson. "The Flux of Iron from Continental Shelf Sediments: A Missing Source for Global Budgets." *Geophysical Research Letters* 31, no. 12 (2004): n/a-n/a.
- Ettwig, Katharina F., Margaret K. Butler, Denis Le Paslier, Eric Pelletier, Sophie Mangenot, Marcel M. M. Kuypers, Frank Schreiber, Bas E. Dutilh, Johannes Zedelius, Dirk de Beer, Jolein Gloerich, Hans J. C. T. Wessels, Theo van Alen, Francisca Luesken, Ming L. Wu, Katinka T. van de Pas-Schoonen, Huub J. M. Op den Camp, Eva M. Janssen-Megens, Kees-Jan Francoijs, Henk Stunnenberg, Jean Weissenbach, Mike S. M. Jetten, and Marc Strous. "Nitrite-Driven Anaerobic Methane Oxidation by Oxygenic Bacteria." *Nature* 464, no. 7288 (2010): 543-548.
- Fossing, H., VA Gallardo, BB Jorgensen, M Hiittel, LP Nielsen, H Schulz, JK Gundersen, J Kiiver, NB Ramsing, and A Teske. "Of Nitrate by the Mat-Forming Sulphur Bacterium Thioploca." *Nature* 374, (1995): 20.
- Froelich, P. N., G. P. Klinkhammer, M. L. Bender, N. A. Luedtke, G. R. Heath, Doug Cullen, Paul Dauphin, Doug Hammond, Blayne Hartman, and Val Maynard. "Early Oxidation of Organic Matter in Pelagic Sediments of the Eastern Equatorial Atlantic: Suboxic Diagenesis." *Geochimica et Cosmochimica Acta* 43, no. 7 (1979): 1075-1090.
- Hansel, Colleen M., Shawn G. Benner, and Scott Fendorf. "Competing Fe(II)-Induced Mineralization Pathways of Ferrihydrite." *Environ Sci Technol* 39, no. 18 (2005): 7147-7153.
- Hou, Lijun, Min Liu, Stephen A. Carini, and Wayne S. Gardner. "Transformation and Fate of Nitrate near the Sediment–Water Interface of Copano Bay." *Continental Shelf Research* 35, (2012): 86-94.
- Huang, S., and P. R. Jaffé. "Characterization of Incubation Experiments and Development of an Enrichment Culture Capable of Ammonium Oxidation under Iron-Reducing Conditions." *Biogeosciences* 12, no. 3 (2015): 769-779.
- Hulth, Stefan, Robert C. Aller, and Franck Gilbert. "Coupled Anoxic Nitrification/Manganese Reduction in Marine Sediments." *Geochimica et Cosmochimica Acta* 63, no. 1 (1998): 49-66.
- Hyacinthe, C., P. Anschutz, P. Carbonel, J. M. Jouanneau, and F. J. Jorissen. "Early Diagenetic Processes in the Muddy Sediments of the Bay of Biscay." *Marine Geology* 177, no. 1–2 (2001): 111-128.
- Jaeschke, Andrea, Ben Abbas, Matthias Zabel, Ellen C. Hopmans, Stefan Schouten, and Jaap S. Sinninghe Damsté. "Molecular Evidence for Anaerobic Ammonium-Oxidizing (Anammox) Bacteria in Continental Shelf and Slope Sediments Off Northwest Africa." *Limnology and Oceanography* 55, no. 1 (2010): 365-376.

- Jaeschke, Andrea, Christine Rooks, Mark Trimmer, Joanna C. Nicholls, Ellen C. Hopmans, Stefan Schouten, and Jaap S. Sinninghe Damsté. "Comparison of Ladderane Phospholipid and Core Lipids as Indicators for Anaerobic Ammonium Oxidation (Anammox) in Marine Sediments." *Geochimica et Cosmochimica Acta* 73, no. 7 (2009): 2077-2088.
- Javanaud, C., V. Michotey, S. Guasco, N. Garcia, P. Anschutz, M. Canton, and P. Bonin. "Anaerobic Ammonium Oxidation Mediated by Mn-Oxides: From Sediment to Strain Level." *Res Microbiol* 162, no. 9 (2011): 848-57.
- Jegou, I., B. Savoye, C. Pirmez, and L. Droz. "Channel-Mouth Lobe Complex of the Recent Amazon Fan: The Missing Piece." *Marine Geology* 252, no. 1-2 (2008): 62-77.
- Johnson, James W., Eric H. Oelkers, and Harold C. Helgeson. "Supcrt92: A Software Package for Calculating the Standard Molal Thermodynamic Properties of Minerals, Gases, Aqueous Species, and Reactions from 1 to 5000 Bar and 0 to 1000°C." *Computers & Geosciences* 18, no. 7 (1992): 899-947.
- Kampschreur, M. J., R. Kleerebezem, Wwm de Vet, and M. C. M. van Loosdrecht. "Reduced Iron Induced Nitric Oxide and Nitrous Oxide Emission." *Water Research* 45, no. 18 (2011): 5945-5952.
- Klueglein, N., and A. Kappler. "Abiotic Oxidation of Fe(II) by Reactive Nitrogen Species in Cultures of the Nitrate-Reducing Fe(II) Oxidizer Acidovorax Sp. Bofen1 - Questioning the Existence of Enzymatic Fe(II) Oxidation (Vol 11, Pg 180, 2013)." *Geobiology* 11, no. 4 (2013): 396-396.
- Koretsky, CarlaM, CharlesM Moore, KristineL Lowe, Christof Meile, ThomasJ DiChristina, and Philippe Van Cappellen. "Seasonal Oscillation of Microbial Iron and Sulfate Reduction in Saltmarsh Sediments (Sapelo Island, Ga, USA)." *Biogeochemistry* 64, no. 2 (2003): 179-203.
- Kostka, Joel E., and George W. Luther Iii. "Partitioning and Speciation of Solid Phase Iron in Saltmarsh Sediments." *Geochimica et Cosmochimica Acta* 58, no. 7 (1994): 1701-1710.
- Kristine L. Lowe, Thomas J. Dichristina Alakendra N. Roychoudhury Philippe Van Cappellen. "Microbiological and Geochemical Characterization of Microbial Fe(II) Reduction in Salt Marsh Sediments." *Geomicrobiology Journal* 17, no. 2 (2000): 163-178.
- Li, Xiaofei, Lijun Hou, Min Liu, Yanling Zheng, Guoyu Yin, Xianbiao Lin, Lv Cheng, Ye Li, and Xiaoting Hu. "Evidence of Nitrogen Loss from Anaerobic Ammonium Oxidation Coupled with Ferric Iron Reduction in an Intertidal Wetland." *Environ Sci Technol* 49, no. 19 (2015): 11560-11568.
- Lin, Hui, and Martial Taillefert. "Key Geochemical Factors Regulating Mn(IV)-Catalyzed Anaerobic Nitrification in Coastal Marine Sediments." *Geochimica et Cosmochimica Acta* 133, (2014): 17-33.
- Lovley, Derek R., and Elizabeth J. P. Phillips. "Rapid Assay for Microbially Reducible Ferric Iron in Aquatic Sediments." *Appl Environ Microbiol* 53, no. 7 (1987): 1536-1540.

- Luther, George W., B. Sundby, B. L. Lewis, P.J. Brendel, and N. Silverberg. "Interactions of Manganese with the Nitrogen Cycle: Alternative Pathways to Dinitrogen." *Geochimica et Cosmochimica Acta* 61, no. 19 (1997): 4043-4052.
- Luther, George W., III. "The Role of One- and Two-Electron Transfer Reactions in Forming Thermodynamically Unstable Intermediates as Barriers in Multi-Electron Redox Reactions." *Aquatic Geochemistry* 16, no. 3 (2010): 395-420.
- Luther, George W., III., Brian T. Glazer, Shufen Ma, Robert E. Trouwborst, Tommy S. Moore, Edouard Metzger, Chareonkwan Kraiya, Tim J. Waite, Gregory Druschel, Bjørn Sundby, Martial Taillefert, Donald B. Nuzzio, Timothy M. Shank, Brent L. Lewis, and Paul J. Brendel. "Use of Voltammetric Solid-State (Micro)Electrodes for Studying Biogeochemical Processes: Laboratory Measurements to Real Time Measurements with an in Situ Electrochemical Analyzer (Isea)." *Marine Chemistry* 108, no. 3-4 (2008): 221-235.
- McKee, B. A., R. C. Aller, M. A. Allison, T. S. Bianchi, and G. C. Kineke. "Transport and Transformation of Dissolved and Particulate Materials on Continental Margins Influenced by Major Rivers: Benthic Boundary Layer and Seabed Processes." *Continental Shelf Research* 24, no. 7-8 (2004): 899-926.
- Meiggs, Deidre, and Martial Taillefert. "The Effect of Riverine Discharge on Biogeochemical Processes in Estuarine Sediments." *Limnology and Oceanography* 56, no. 5 (2011): 1797-1810.
- Millero, Frank J., and Donald R. Schreiber. "Use of the Ion Pairing Model to Estimate Activity Coefficients of the Ionic Components of Natural Waters." *American Journal of Science* 282, (1982): 33.
- Milucka, J., T. G. Ferdelman, L. Polerecky, D. Franzke, G. Wegener, M. Schmid, I. Lieberwirth, M. Wagner, F. Widdel, and M. M. Kuypers. "Zero-Valent Sulphur Is a Key Intermediate in Marine Methane Oxidation." *Nature* 491, no. 7425 (2012): 541-6.
- Morel, F. M. M., J. G. Rueter, Donald M. Anderson, and R. R. L. Guillard. "Aquil: A Chemically Defined Phytoplankton Culture Medium for Trace Metal Studies." *Journal of Phycology* 15, no. 2 (1979): 135-141.
- Mulder, A., A. A. van de Graaf, L. A. Robertson, and J. G. Kuenen. "Anaerobic Ammonium Oxidation Discovered in a Denitrifying Fluidized Bed Reactor." *FEMS Microbiology Ecology* 16, no. 3 (1995): 177-184.
- Park, Wooshin, Youn-Ku Nam, Myun-Joo Lee, and Tak-Hyun Kim. "Anaerobic Ammonia-Oxidation Coupled with Fe³⁺ Reduction by an Anaerobic Culture from a Piggery Wastewater Acclimated to NH₄⁺/Fe³⁺ Medium." *Biotechnology and Bioprocess Engineering* 14, no. 5 (2009): 680-685.
- Pedersen, Hanne D., Dieke Postma, Rasmus Jakobsen, and Ole Larsen. "Fast Transformation of Iron Oxyhydroxides by the Catalytic Action of Aqueous Fe(II)." *Geochimica et Cosmochimica Acta* 69, no. 16 (2005): 3967-3977.

- Poulton, S. W., and D. E. Canfield. "Development of a Sequential Extraction Procedure for Iron: Implications for Iron Partitioning in Continentally Derived Particulates." *Chemical Geology* 214, no. 3-4 (2005): 209-221.
- Poulton, Simon W., and Robert Raiswell. "Chemical and Physical Characteristics of Iron Oxides in Riverine and Glacial Meltwater Sediments." *Chemical Geology* 218, no. 3-4 (2005): 203-221.
- Rabouille, C., J. C. Caprais, B. Lansard, P. Crassous, K. Dedieu, J. L. Reyss, and A. Khripounoff. "Organic Matter Budget in the Southeast Atlantic Continental Margin Close to the Congo Canyon: In Situ Measurements of Sediment Oxygen Consumption." *Deep-Sea Research Part II-Topical Studies in Oceanography* 56, no. 23 (2009): 2223-2238.
- Raimonet, Mélanie, Olivier Ragueneau, Vincent Jacques, Rudolph Corvaisier, Brivaëla Moriceau, Alexis Khripounoff, Lara Pozzato, and Christophe Rabouille. "Rapid Transport and High Accumulation of Amorphous Silica in the Congo Deep-Sea Fan: A Preliminary Budget." *Journal of Marine Systems* 141, (2015): 71-79.
- Rickard, David. "The Solubility of FeS." *Geochimica et Cosmochimica Acta* 70, no. 23 (2006): 5779-5789.
- Rickard, David, and George W. Luther III. "Kinetics of Pyrite Formation by the H₂S Oxidation of Iron (II) Monosulfide in Aqueous Solutions between 25 and 125°C: The Mechanism." *Geochimica et Cosmochimica Acta* 61, no. 1 (1997): 135-147.
- Riedinger, N., M. J. Formolo, T. W. Lyons, S. Henkel, A. Beck, and S. Kasten. "An Inorganic Geochemical Argument for Coupled Anaerobic Oxidation of Methane and Iron Reduction in Marine Sediments." *Geobiology* 12, no. 2 (2014): 172-181.
- Rooks, Christine, Markus C. Schmid, Wahida Mehsana, and Mark Trimmer. "The Depth-Specific Significance and Relative Abundance of Anaerobic Ammonium-Oxidizing Bacteria in Estuarine Sediments (Medway Estuary, UK)." *FEMS Microbiology Ecology* 80, no. 1 (2012): 19-29.
- Rysgaard, Søren, and Ronnie Nøhr Glud. "Anaerobic N₂ Production in Arctic Sea Ice." *Limnology and Oceanography* 49, no. 1 (2004): 86-94.
- Savoie, Bruno, Nathalie Babonneau, Bernard Dennielou, and Martine Bez. "Geological Overview of the Angola-Congo Margin, the Congo Deep-Sea Fan and Its Submarine Valleys." *Deep Sea Research Part II: Topical Studies in Oceanography* 56, no. 23 (2009): 2169-2182.
- Sawayama, Shigeki. "Possibility of Anoxic Ferric Ammonium Oxidation." *Journal of Bioscience and Bioengineering* 101, no. 1 (2006): 70-72.
- Sayama, Mikio. "Presence of Nitrate-Accumulating Sulfur Bacteria and Their Influence on Nitrogen Cycling in a Shallow Coastal Marine Sediment." *Appl Environ Microbiol* 67, no. 8 (2001): 3481-3487.

- Schippers, Axel, and Bo Barker Jørgensen. "Biogeochemistry of Pyrite and Iron Sulfide Oxidation in Marine Sediments." *Geochimica et Cosmochimica Acta* 66, no. 1 (2002): 85-92.
- Schulz, H. N., T. Brinkhoff, T. G. Ferdelman, M. Hernández Mariné, A. Teske, and B. B. Jørgensen. "Dense Populations of a Giant Sulfur Bacterium in Namibian Shelf Sediments." *Science* 284, no. 5413 (1999): 493-495.
- Severmann, Silke, Clark M. Johnson, Brian L. Beard, and James McManus. "The Effect of Early Diagenesis on the Fe Isotope Compositions of Porewaters and Authigenic Minerals in Continental Margin Sediments." *Geochimica et Cosmochimica Acta* 70, no. 8 (2006): 2006-2022.
- Silver, Whendee L., Donald J. Herman, and Mary K. Firestone. "Dissimilatory Nitrate Reduction to Ammonium in Upland Tropical Forest Soils." *Ecology* 82, no. 9 (2001): 2410-2416.
- Sørensen, Jan. "Capacity for Denitrification and Reduction of Nitrate to Ammonia in a Coastal Marine Sediment." *Appl Environ Microbiol* 35, no. 2 (1978): 301-305.
- _____. "Reduction of Ferric Iron in Anaerobic, Marine Sediment and Interaction with Reduction of Nitrate and Sulfate." *Appl Environ Microbiol* 43, no. 2 (1982): 319-324.
- Straub, K L, M Benz, B Schink, and F Widdel. "Anaerobic, Nitrate-Dependent Microbial Oxidation of Ferrous Iron." *Appl Environ Microbiol* 62, no. 4 (1996): 1458-60.
- Strous, M., J. G. Kuenen, and M. S. M. Jetten. "Key Physiology of Anaerobic Ammonium Oxidation." *Appl Environ Microbiol* 65, no. 7 (1999): 3248-3250.
- Stumm, W., and J.J. Morgan. *Aquatic Chemistry: Chemical Equilibria and Rates in Natural Waters*: Wiley, 1996.
- Taillefert, Martial, George W. Luther, and Donald B. Nuzzio. "The Application of Electrochemical Tools for in Situ Measurements in Aquatic Systems." *Electroanalysis* 12, no. 6 (2000): 401-412.
- Taillefert, Martial, Stephanie Neuhuber, and Gwendolyn Bristow. "The Effect of Tidal Forcing on Biogeochemical Processes in Intertidal Salt Marsh Sediments." *Geochemical Transactions* 8, no. 1 (2007): 6.
- Thamdrup, B. "New Pathways and Processes in the Global Nitrogen Cycle." In *Annual Review of Ecology, Evolution, and Systematics, Vol 43*, edited by D. J. Futuyma, 43, 407-428, 2012.
- Thamdrup, Bo, and Tage Dalsgaard. "The Fate of Ammonium in Anoxic Manganese Oxide-Rich Marine Sediment." *Geochimica et Cosmochimica Acta* 64, no. 24 (2000): 4157-4164.
- _____. "Production of N₂ through Anaerobic Ammonium Oxidation Coupled to Nitrate Reduction in Marine Sediments." *Appl Environ Microbiol* 68, no. 3 (2002): 1312-1318.

- Thorneley, Roger N. F., Robert R. Eady, and David J. Lowe. "Biological Nitrogen Fixation by Way of an Enzyme-Bound Dinitrogen-Hydride Intermediate." *Nature* 272, no. 5653 (1978): 557-558.
- Van Cleemput, O., and L. Baert. "Nitrite Stability Influenced by Iron Compounds." *Soil Biology and Biochemistry* 15, no. 2 (1983): 137-140.
- van der Zee, Claar, Darryl R. Roberts, Denis G. Rancourt, and Caroline P. Slomp. "Nanogoethite Is the Dominant Reactive Oxyhydroxide Phase in Lake and Marine Sediments." *Geology* 31, no. 11 (2003): 993-996.
- Van Genuchten, Martinus Th. "Analytical Solutions for Chemical Transport with Simultaneous Adsorption, Zero-Order Production and First-Order Decay." *Journal of Hydrology* 49, no. 3-4 (1981): 213-233.
- Wang, Yifeng, and Philippe Van Cappellen. "A Multicomponent Reactive Transport Model of Early Diagenesis: Application to Redox Cycling in Coastal Marine Sediments." *Geochimica et Cosmochimica Acta* 60, no. 16 (1996): 2993-3014.
- Weber, Karrie A., Jarrod Pollock, Kimberly A. Cole, Susan M. O'Connor, Laurie A. Achenbach, and John D. Coates. "Anaerobic Nitrate-Dependent Iron(II) Bio-Oxidation by a Novel Lithoautotrophic Betaproteobacterium, Strain 2002." *Appl Environ Microbiol* 72, no. 1 (2006): 686-694.
- Weber, KarrieA, DavidB Hedrick, AaronD Peacock, J. Cameron Thrash, DavidC White, LaurieA Achenbach, and JohnD Coates. "Physiological and Taxonomic Description of the Novel Autotrophic, Metal Oxidizing Bacterium, Pseudogulbenkiania Sp. Strain 2002." *Applied Microbiology and Biotechnology* 83, no. 3 (2009): 555-565.
- Wehrmann, Laura M., Michael J. Formolo, Jeremy D. Owens, Robert Raiswell, Timothy G. Ferdelman, Natascha Riedinger, and Timothy W. Lyons. "Iron and Manganese Speciation and Cycling in Glacially Influenced High-Latitude Fjord Sediments (West Spitsbergen, Svalbard): Evidence for a Benthic Recycling-Transport Mechanism." *Geochimica et Cosmochimica Acta* 141, (2014): 628-655.
- Wu, Wenfang, Bi Li, Jing Hu, Jinhua Li, Fengping Wang, and Yongxin Pan. "Iron Reduction and Magnetite Biomineralization Mediated by a Deep-Sea Iron-Reducing Bacterium *Shewanella piezotolerans* Wp3." *Journal of Geophysical Research: Biogeosciences (2005-2012)* 116, no. G4 (2011).
- Yang, Wendy H., Karrie A. Weber, and Whendee L. Silver. "Nitrogen Loss from Soil through Anaerobic Ammonium Oxidation Coupled to Iron Reduction." *Nature Geosci* 5, no. 8 (2012): 538-541.
- Zachara, John M., Ravi K. Kukkadapu, James K. Fredrickson, Yuri A. Gorby, and Steven C. Smith. "Biomineralization of Poorly Crystalline Fe(III) Oxides by Dissimilatory Metal Reducing Bacteria (Dmrb)." *Geomicrobiology Journal* 19, no. 2 (2002): 179-207.

Zhao, Linduo, Hailiang Dong, Ravi Kukkadapu, Abinash Agrawal, Deng Liu, Jing Zhang, and Richard E. Edlmann. "Biological Oxidation of Fe(I) in Reduced Nontronite Coupled with Nitrate Reduction by Pseudogulbenkiania Sp. Strain 2002." *Geochimica et Cosmochimica Acta* 119, (2013): 231-247.

